Electronic Supplementary Information for

Refined molecular microstructure and optimized carrier management of multicomponent organic photovoltaics toward 19.3% certified efficiency

Shuixing Li,‡[a] Chengliang He,‡[a] Tianyi Chen,‡[a] Jiale Zheng,‡[b] Rui Sun,[c] Jin Fang,[d] Yiyao Chen,[e] Youwen Pan,[a] Kangrong Yan,[a] Chang-Zhi Li,[a] Minmin Shi,[a] Lijian Zuo,[a] Chang-Qi Ma,[d] Jie Min,[c] Yujing Liu*[b] and Hongzheng Chen*[a]

[a] State Key Laboratory of Silicon Materials, International Research Center for X Polymers, Department of Polymer Science and Engineering, Zhejiang University, Hangzhou 310027, P. R. China.
Email: hzchen@zju.edu.cn
[b] College of Materials Science and Engineering, Zhejiang University of Technology, Hangzhou 310014, P. R. China.
Email: yujingliu@zjut.edu.cn
[c] The Institute for Advanced Studies, Wuhan University, Wuhan 430072, P. R. China.
[d] i-Lab & Printable Electronics Research Centre, Suzhou Institute of Nano-tech and Nano-bionics, Chinese Academy of Sciences, Suzhou 215123, P. R. China.
[e] Vacuum Interconnected Nanotech Workstation (Nano-X), Suzhou Institute of Nano-Tech and Nano-Bionics, Chinese Academy of Sciences, Suzhou 215123, P. R. China.
‡ S. Li, C. He, T. Chen and J. Zheng contributed equally to this work.

Supplementary Experimental Procedures

Materials

Polymer donor PM6 was purchased from Solarmer Materials. The other reagents and chemicals were purchased from commercial sources and used as received. BTP-S2 (*Adv. Mater.* **2020**, *32*, 2001160) and BTP-S9 (*Nat. Commun.* **2021**, *12*, 4627) were synthesized according to our previous reported work. The detailed synthetic procedures of BTP-S11, BTP-S12 and BTP-S15 are described below.

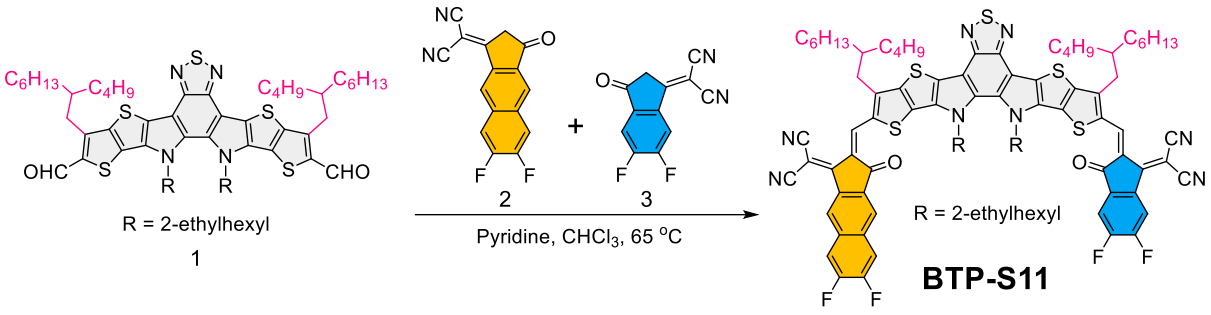

2-((Z)-2-((3,9-bis(2-butyloctyl)-10-(((Z)-1-(dicyanomethylene)-5,6-difluoro-3-oxo-1,3-dihydro-2H-inden-2-ylidene)methyl)-12,13-bis(2-ethylhexyl)-12,13-dihydro-[1,2,5]thiadiazolo[3,4-e]thieno[2'',3'':4',5']thieno[2',3':4,5]pyrrolo[3,2-g]thieno[2',3':4,5]thieno[3,2-b]indol-2-yl)methylene)-6,7-difluoro-3-oxo-2,3-dihydro-1H-cyclopenta[b]naphthalen-1-ylidene)malononitrile (**BTP-S11**)

To a Schlenk tube were added **Compound 1** (0.4 g, 0.38 mmol), **Compound 2** (0.22 g, 0.8 mmol), **Compound 3** (0.18 g, 0.8 mmol) and $CHCl_3$ (50 mL). The mixture was frozen with liquid nitrogen, followed by three times of successive vacuum and nitrogen fill cycles. Under the protection of N_2, 1 mL pyridine was injected. Then, the reactant was refluxed at 65 °C for 22 h. The crude product was purified using silica gel column chromatography with the mixture of petroleum ether and dichloromethane (1:1, v/v) as the eluent, yielding a deep brown solid (0.20 g, 34%). ^{1}H NMR (500 MHz, CDCl3): δ = 9.21 (s, 1H), 9.14 (s, 1H), 9.10 (s, 1H), 8.56 (dd, *J* = 9.9, 6.5 Hz, 1H), 8.30 (s, 1H), 7.80 (dd, J = 18.1, 10.3 Hz, 2H), 7.71 (t, *J* = 7.4 Hz, 1H), 4.81 (t, *J* = 7.3 Hz, 4H), 3.16 (t, *J* = 6.7 Hz, 4H), 2.17-2.03 (m, 4H), 1.52-1.43 (m, 4H), 1.41-1.34 (m, 4H), 1.32-0.92 (m, 40H), 0.89-0.75 (m, 18H), 0.71-0.63 (m, 6H). MS (MALDI-TOF): Cald for $C_{88}H_{92}F_4N_8O_2S_5$ (M^+): 1530.05, Found: 1530.09.

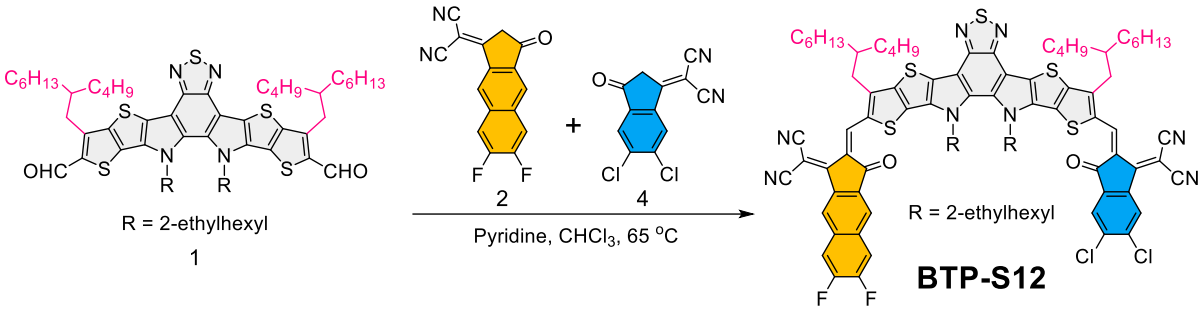

2-((Z)-2-((3,9-bis(2-butyloctyl)-10-(((Z)-5,6-dichloro-1-(dicyanomethylene)-3-oxo-1,3-dihydro-2H-inden-2-ylidene)methyl)-12,13-bis(2-ethylhexyl)-12,13-dihydro-[1,2,5]thiadiazolo[3,4-e]thieno[2'',3'':4',5']thieno[2',3':4,5]pyrrolo[3,2-g]thieno[2',3':4,5]thieno[3,2-b]indol-2-yl)methylene)-6,7-difluoro-3-oxo-2,3-dihydro-1H-cyclopenta[b]naphthalen-1-ylidene)malononitrile (**BTP-S12**)

To a Schlenk tube were added **Compound 1** (0.53 g, 0.5 mmol), **Compound 2** (0.28 g, 1 mmol), **Compound 4** (0.26 g, 1 mmol) and $CHCl_3$ (50 mL). The mixture was frozen with liquid nitrogen, followed by three times of successive vacuum and nitrogen fill cycles. Under the protection of N_2, 1 mL pyridine was injected. Then, the reactant was refluxed at 65 °C for 22 h. The crude product was purified using silica gel column chromatography with the mixture of petroleum ether and dichloromethane (1:1, v/v) as the eluent, yielding a deep brown solid (0.19 g, 24%). ^{1}H NMR (500 MHz, CDCl3): δ = 9.25 (s, 1H), 9.17 (s, 1H), 9.13 (s, 1H), 8.80 (s, 1H), 8.33 (s, 1H), 7.98 (s, 1H), 7.87-7.78 (m, 2H), 4.79 (t, *J* = 6.8 Hz, 4H), 3.20 (dd, *J* = 14.6, 7.8 Hz, 4H), 2.16-2.03 (m, 4H), 1.51-1.43 (m, 4H), 1.42-1.36 (m, 4H), 1.34-0.91 (m, 40H), 0.90-0.72 (m, 18H), 0.70-0.60 (m, 6H). MS (MALDI-TOF): Cald for $C_{88}H_{92}Cl_2F_2N_8O_2S_5$ (M+): 1562.95, Found: 1562.47.

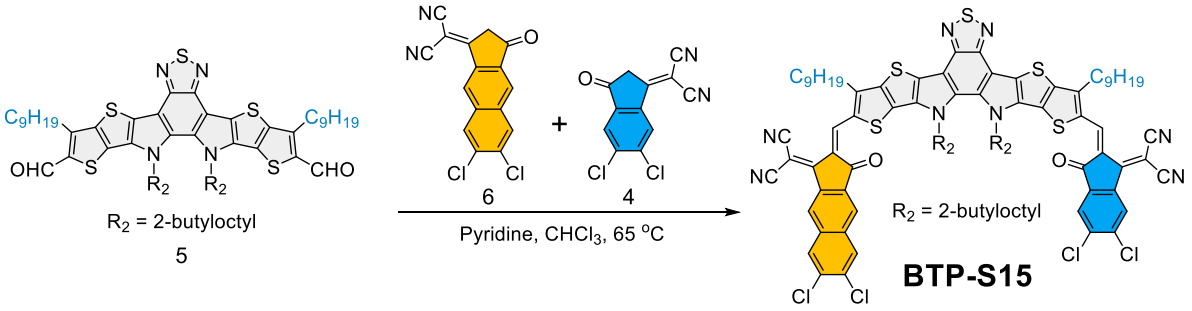

2-((Z)-2-((12,13-bis(2-butyloctyl)-10-(((Z)-5,6-dichloro-1-(dicyanomethylene)-3-oxo-1,3-dihydro-2H-inden-2-ylidene)methyl)-3,9-dinonyl-12,13-dihydro-[1,2,5]thiadiazolo[3,4-e]thieno[2'',3'':4',5']thieno[2',3':4,5]pyrrolo[3,2-g]thieno[2',3':4,5]thieno[3,2-b]indol-2-yl)methylene)-6,7-dichloro-3-oxo-2,3-dihydro-1H-cyclopenta[b]naphthalen-1-ylidene)malononitrile (**BTP-S15**)

To a Schlenk tube were added **Compound 5** (0.27 g, 0.25 mmol), **Compound 4** (0.13 g, 0.5 mmol), **Compound 6** (0.16 g, 0.5 mmol) and $CHCl_3$ (50 mL). The mixture was frozen with liquid nitrogen, followed by three times of successive vacuum and nitrogen fill cycles. Under

the protection of N_2, 0.6 mL pyridine was injected. Then, the reactant was refluxed at 65 °C for 21 h. The crude product was purified using silica gel column chromatography with the mixture of petroleum ether and dichloromethane (1:1, v/v) as the eluent, yielding a black solid (0.09 g, 22%). ^{1}H NMR (500 MHz, CDCl3): δ = 9.17 (d, *J* = 18.2 Hz, 2H), 9.03 (s, 1H), 8.77 (s, 1H), 8.25 (s, 1H), 8.16 (s, 1H), 8.11 (s, 1H), 7.96 (s, 1H), 4.89-4.74 (m, 4H), 3.27-3.11 (m, 4H), 2.22-2.12 (m, 2H), 1.92-1.80 (m, 4H), 1.54-1.47 (m, 4H), 1.42-1.33 (m, 4H), 1.32-1.21 (m, 20H), 1.16-0.84 (m, 34H), 0.74-0.65 (m, 12H). MS (MALDI-TOF): Cald for $C_{90}H_{96}Cl_4N_8O_2S_5$ (M+): 1623.91; Found: 1624.38.

General characterizations

^{1}H NMR spectra were obtained on a Bruker Advance III 500 (500 MHz) nuclear magnetic resonance (NMR) spectroscope. MALDI-TOF MS spectra were measured on a Walters Maldi Q-TOF Premier mass spectrometry. UV-vis-NIR absorption spectra were recorded on a Shimadzu UV-1800 spectrophotometer. Cyclic voltammetry (CV) was done on a CHI600A electrochemical workstation with Pt disk, Pt plate, and standard calomel electrode (SCE) as working electrode, counter electrode, and reference electrode, respectively, in a 0.1 mol/L tetrabutylammoniumhexafluorophosphate (Bu_4NPF_6) acetonitrile solution. The CV curves were recorded versus the potential of SCE, which was calibrated by the ferrocene-ferrocenium (Fc/Fc^+) redox couple (4.8 eV below the vacuum level). The equation of $E_{LUMO/HOMO}$ = -e($E_{red/ox}$+4.41) (eV) was used to calculate the LUMO and HOMO levels (the redox potential of Fc/Fc^+ is found to be 0.39 V). AFM images were obtained on a VeecoMultiMode atomic force microscopy in the tapping mode. Differential scanning calorimetry (DSC) was recorded on a Pekin-Elmer Pyris 1 differential scanning calorimeter. Ultraviolet photoelectron spectroscopy (UPS) data was conducted by an ESCALAB Xi+ system (Thermo Scientific), He I radiation (21.22 eV) with an applied bias of -10 V was used for UPS.

HR-TEM

The HR-TEM was conducted by employing a transfer holder and TEM (FEI Talos-S) at 200 kV. 300 mesh Cu was used as a carrier for the film deposition. All samples were prepared via the spin-coating and annealing process for TEM imaging. At first, the prepared solution (donor: 4 mg/ml, acceptor: 6mg/ml, blend: 8.25 mg/ml) was slowly and evenly dripped onto the Cu mesh, which was placed on spin coater to make the film at the speed of 1000 rpm. Then, the corresponding samples were thermally annealed for 10 min.

EL

The EL signature was collected with a monochromator and detected with an InGaAs detector. Data collection range is 700-1300 nm.

FTPS-EQE

The FTPS measurements were recorded using a Bruker Vertex 70 Fourier-transform infrared (FTIR) spectrometer, equipped with a quartz tungsten halogen lamp, a quartz beam-splitter, and an external detector option. A low noise current amplifier (Femto DLPCA-200) was used to amplify the photocurrent produced on the illumination of the photovoltaic devices with light modulated by the FTIR. The output voltage of the current amplifier was fed back into the external detector port of the FTIR. The photocurrent spectrum was collected by FTIR's software.

EQE_{EL}

Electroluminescence quantum efficiency (EQE_{EL}) measurements were performed by applying

external voltage sources through the devices from 1V to 4V. A Keithley 2400 SourceMeter was used for supplying voltages and recording injected current, and a Keithley 485 picoammeter was used for measuring the emitted light intensity.

GIWAXS

GIWAXS measurements were performed in a Xeuss 3.0 SAXS/WAXS system with a wavelength of λ = 1.542 Å at Vacuum Interconnected Nanotech Workstation (Nano-X).

Device fabrication and measurement

Organic photovoltaics were fabricated on glass substrates commercially pre-coated with a layer of ITO with the conventional structure of ITO/PEDOT:PSS/Active layer/Bis-FIMG/Ag. Prior to fabrication, the substrates were cleaned using detergent, deionized water, acetone and isopropanol consecutively for 15 min in each step, and then treated in an ultraviolet ozone generator for 15 min before being spin coated at 4500 rpm with a layer of 20 nm thick PEDOT:PSS (Baytron P AI4083). After baking the PEDOT:PSS layer in air at 170 ºC for 20 min, the substrates were transferred to a glovebox. The active layer was formed according to the following procedure: the donor and acceptor were dissolved in chloroform solution with a total concentration of 16.5 mg/ml for all active layers, except PM6:BTP-S12, whose total concentration was 12 mg/ml due to the limited solubility of BTP-S12; the donor:acceptor weight ratio was fixed as 1:1.2 for all active layers; after heating the solution at 55 ºC for 1h, the solution was cooled for 3 min and then 0.25% (v/v) DIO was added as the additive; then the solution was further heated at 55 ºC for 10 min, after that, the active layer was spin-coated at

3000-3500 rpm for 25 s, except PM6:BTP-S12, whose spin-coating speed was 1800-2000 rpm for 25 s. Then an extra preannealing at 80 °C for 8 min was performed. A thin layer of Bis-FIMG was spin-coated from 1 mg/ml methanol solution at 4000 rpm for 40 s on the top of active layer. Finally, the Ag (100 nm) electrode was deposited by thermal evaporation to complete the device with an active layer of 6 mm^2, as defined by the overlapping area of ITO and Ag. A mask with an area of 4.73 mm^2 was used to measure the efficiencies. The *J-V* measurement was performed via the solar simulator (SS-F5-3A, Enlitech) along with AM 1.5 G spectra at 100 mW/cm^2, that was calibrated by the certified standard silicon solar cell (SRC-2020, Enlitech) with KG-2 filter. Devices were tested in N_2-filled glovebox. The scan direction is -0.1 to 1 V, with a scan step of 0.01 V and dwell time is 1 ms. The EQE data were obtained by using the solar-cell spectral-response measurement system (RE-R, Enlitech).

SCLC measurement

The charge carrier mobilities of the blend films were measured using the space-charge-limited current method. Hole-only devices were fabricated in a structure of ITO/PEDOT:PSS/Active layer/MoO_3/Ag, electron-only devices were fabricated in a structure of ITO/ZnO/Active layer/Bis-FIMG/Ag. The device characteristics were extracted by modeling the dark current under forward bias using the SCLC expression described by the Mott-Gurney law: $J=9\varepsilon_r\varepsilon_0\mu V^2/8L^3$, where $\varepsilon_r \approx 3$ is the average dielectric constant of the active layer, ε_0 is the permittivity of the free space, μ is the carrier mobility, V is the applied voltage and L is the thickness of the film.

Supplementary Figures and Notes

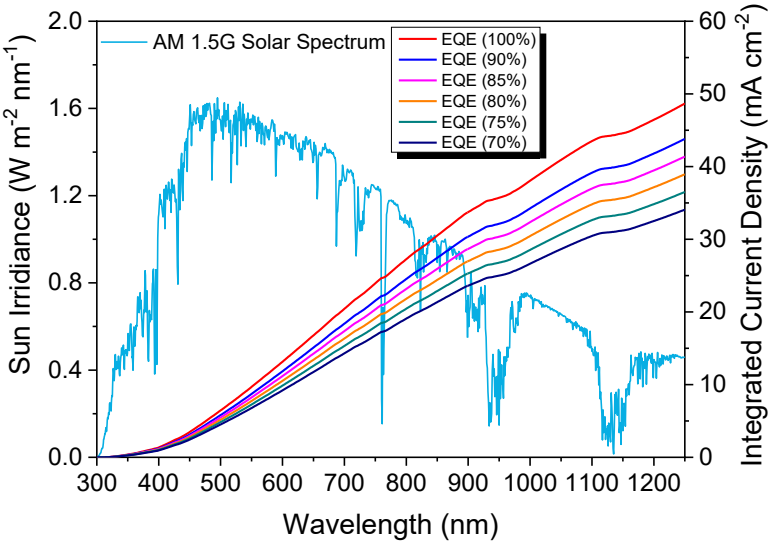

Fig. S1 AM 1.5 G solar spectrum and integrated current density.

Note S1: Theoretical efficiency calculation

For theoretical efficiency calculation, it's performed according to the following procedure:

Firstly, wavelength (or bandgap E_g) and energy loss (E_{loss}) are set as two variates, which are strongly correlated with the photovoltaic materials. The efficiency matrix figure will be formed by calculating enough single dots. Here, we set the wavelength ranging from 700 to 1000 nm and energy loss ranging from 0.6 to 0.3 eV, and 30100 single efficiency dots are calculated.

Secondly, for the calculation of single efficiency dot, voltage (V_{oc}) is obtained via the following equation (1):

$$V_{oc} = \frac{E_g - E_{loss}}{q} \qquad (1)$$

Photocurrent (J_{sc}) is calculated via the following equation (2):

$$J_{sc} = q \cdot \int_0^{\infty} N_{\lambda}(\lambda) \cdot EQE(\lambda) d\lambda \qquad (2)$$

where N_{λ} is the photon flux spectrum of the AM 1.5 G solar spectrum. The results of integrated current densities with various EQE values are shown in above **Fig. S1**. For fill factor (FF), we can either set it as a fixed value or use the max value calculated through the following empirical equation (3):

$$FF = \frac{\gamma_{oc} - \ln(\gamma_{oc} + 0.72)}{\gamma_{oc} + 1} \qquad (3)$$

where γ_{oc} is the normalized V_{oc}, and can be obtained with the following equation (4):

$$\gamma_{oc} = e\, V_{oc} / n\, kT \qquad (4)$$

where e is the elementary charge, n is the diode ideality factor (for high-efficiency OPVs, n ≈ 1), k is Boltzmann constant and T is the temperature.

Finally, the power conversion efficiency (PCE) for a single dot with a specific combination of wavelength and energy loss can be calculated through the following equation (5):

$$PCE = \frac{V_{oc} \times J_{sc} \times FF}{P_{in}} \qquad (5)$$

where P_{in} is the input light power density of the AM 1.5 G solar light.

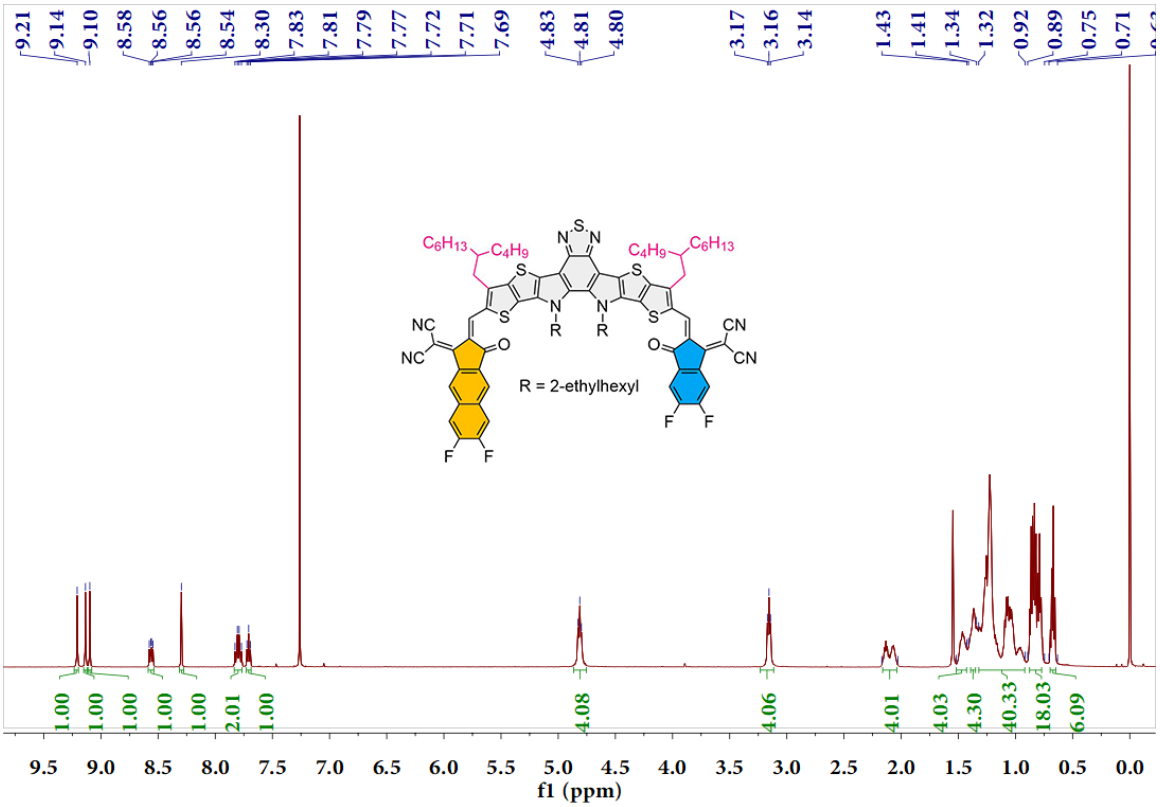

Fig. S2 ^{1}H NMR spectrum of BTP-S11.

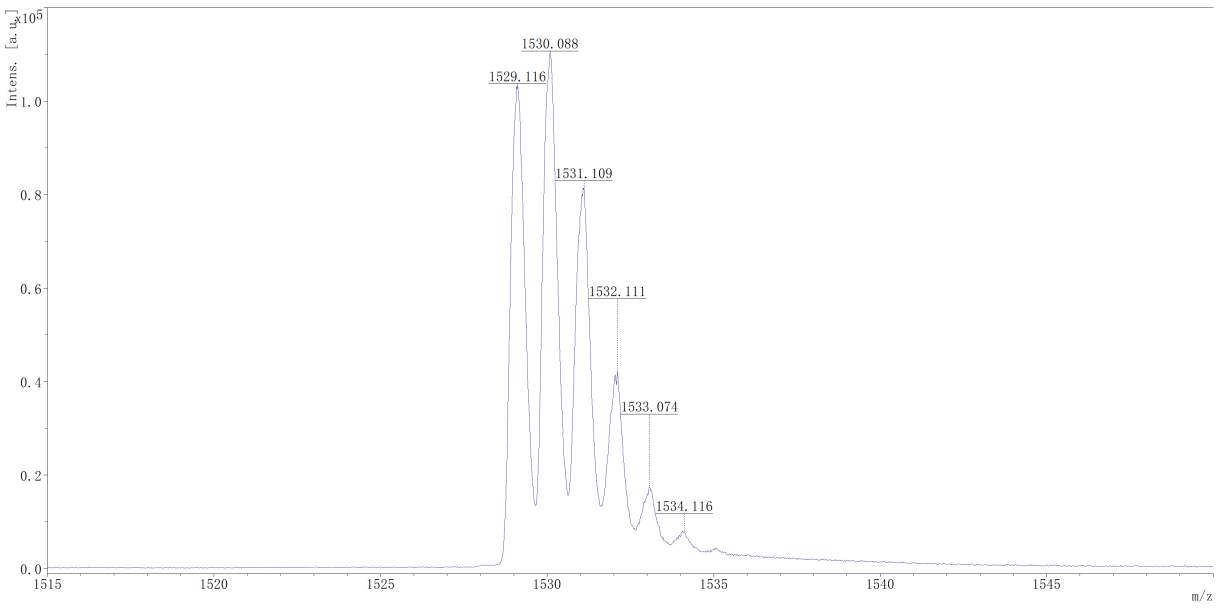

Fig. S3 MALDI-TOF mass spectrum of BTP-S11.

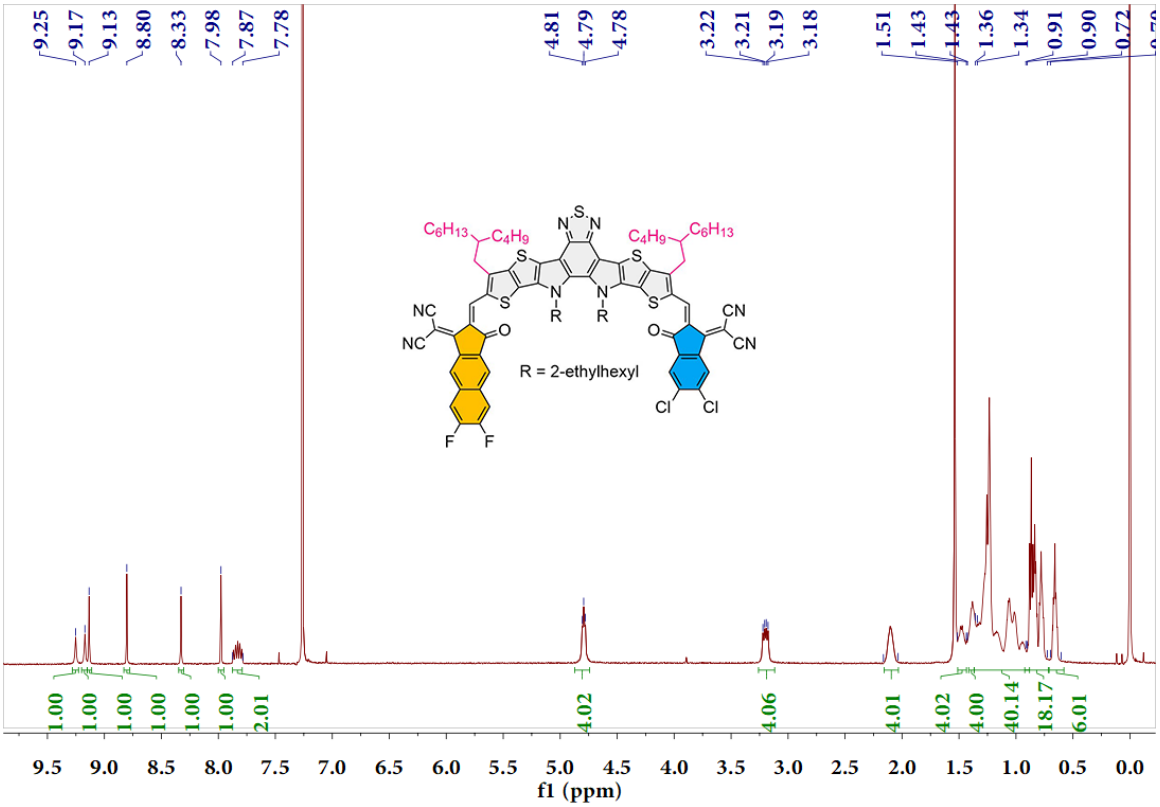

Fig. S4 ^{1}H NMR spectrum of BTP-S12.

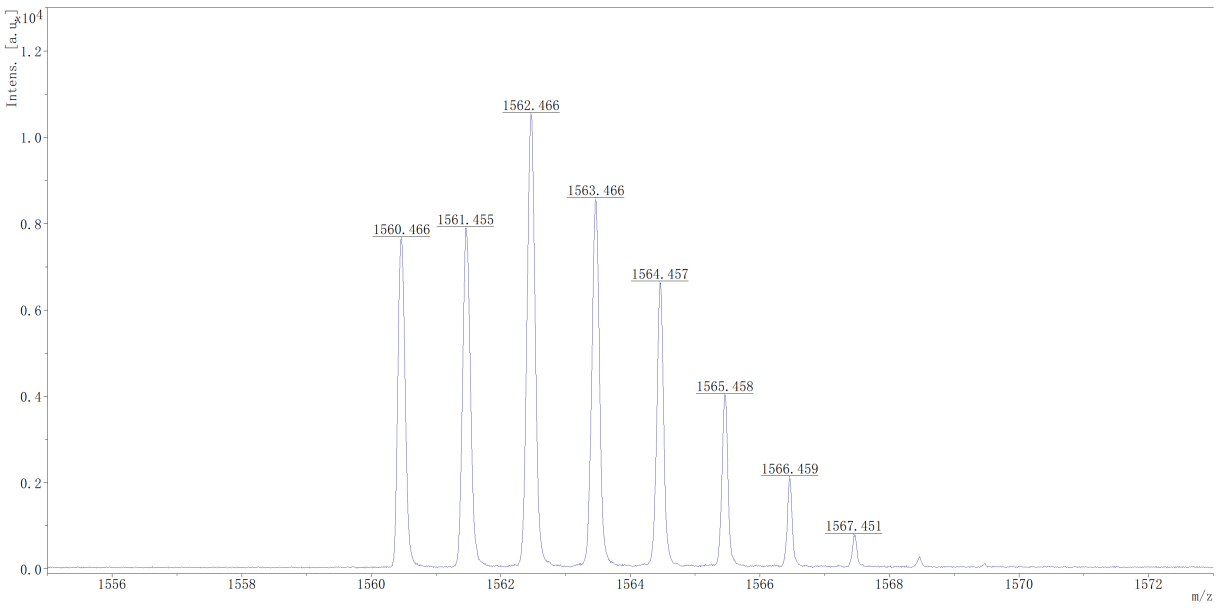

Fig. S5 MALDI-TOF mass spectrum of BTP-S12.

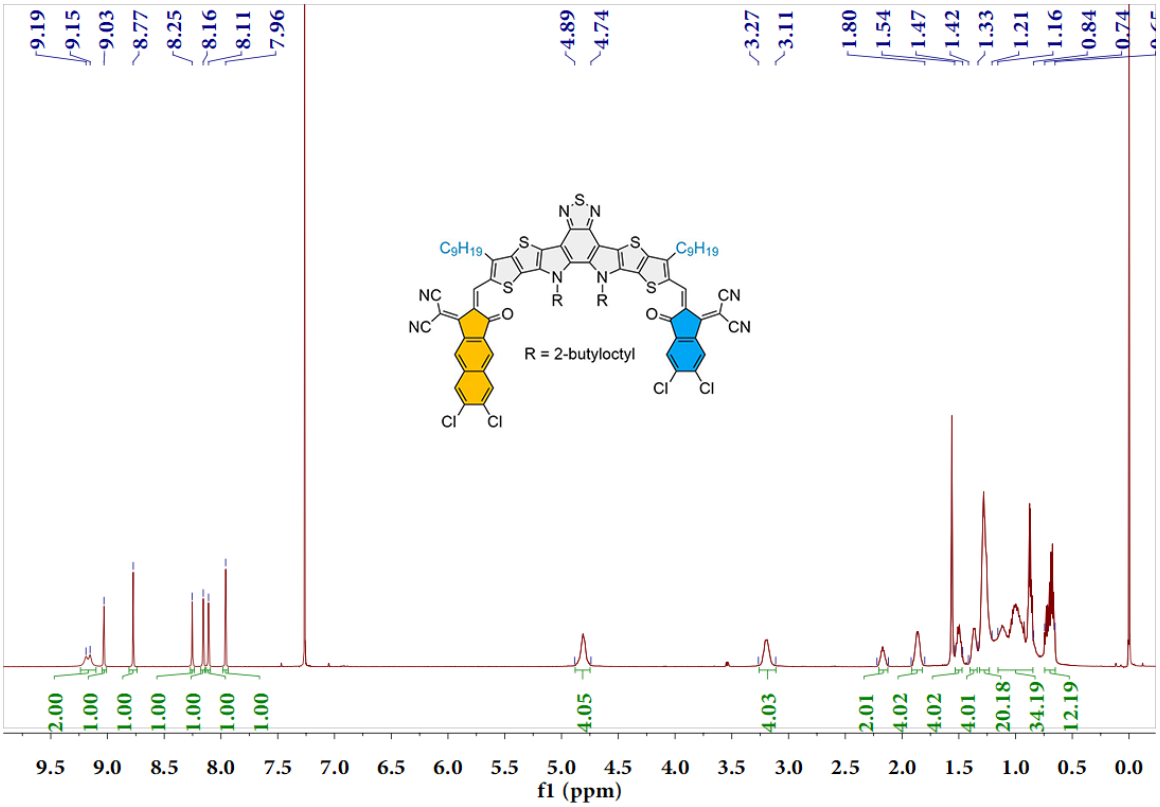

Fig. S6 ^{1}H NMR spectrum of BTP-S15.

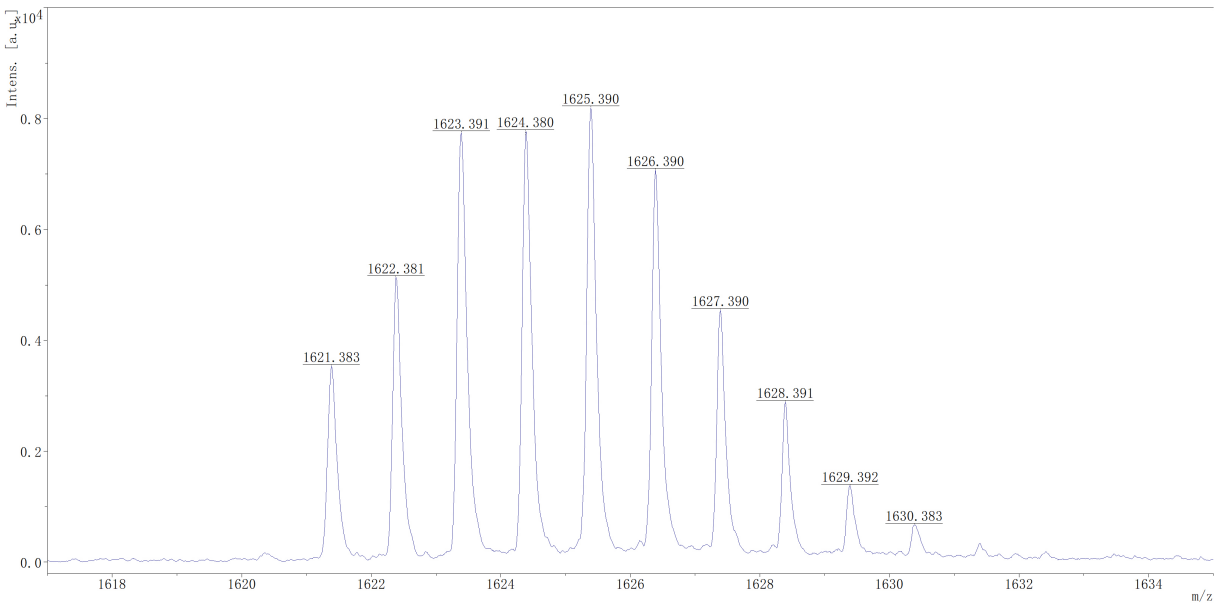

Fig. S7 MALDI-TOF mass spectrum of BTP-S15.

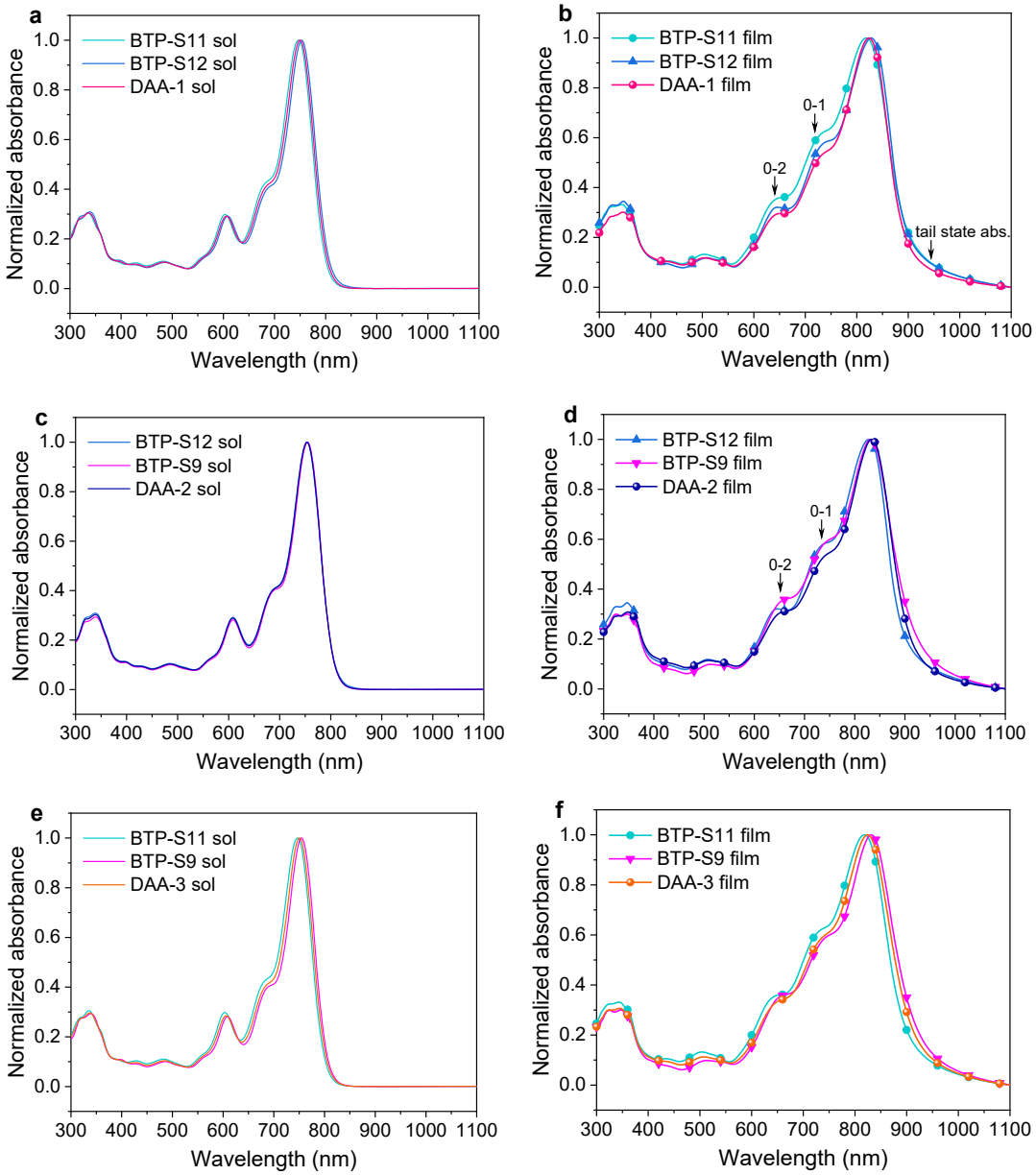

Fig. S8 (a-b) Normalized absorption spectra of BTP-S11, BTP-S12 and DAA-1 in chloroform solutions and films. (c-d) Normalized absorption spectra of BTP-S12, BTP-S9 and DAA-2 in chloroform solutions and films. (e-f) Normalized absorption spectra of BTP-S11, BTP-S9 and DAA-3 in chloroform solutions and films.

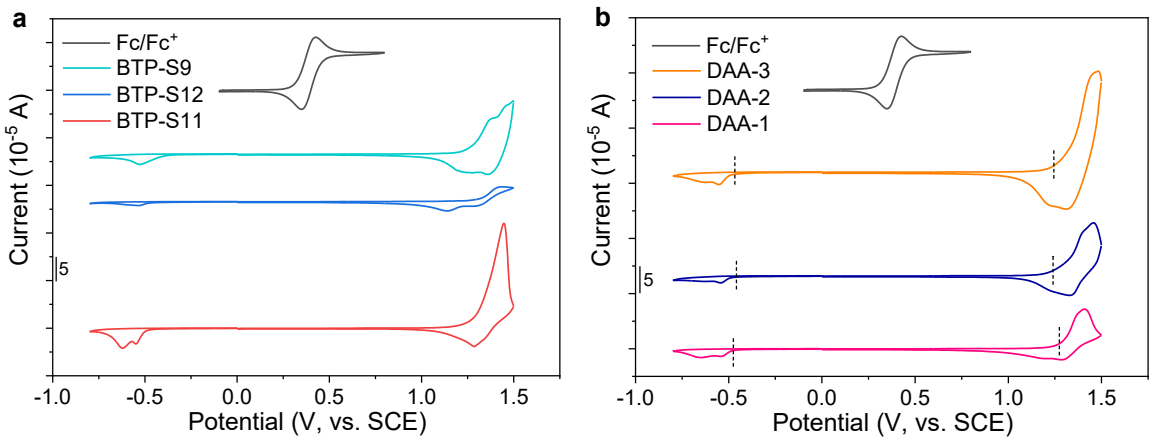

Fig. S9 (a) Cyclic voltammograms of BTP-S11, BTP-S12 and BTP-S9. (b) Cyclic voltammograms of DAA-1, DAA-2 and DAA-3.

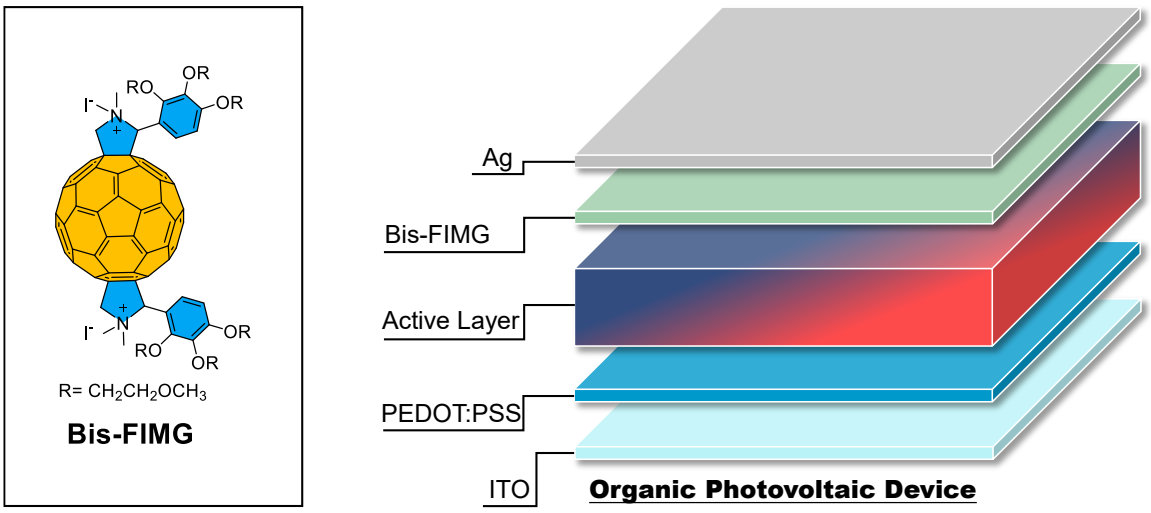

Fig. S10 Chemical structure of Bis-FIMG and device structure of OPVs.

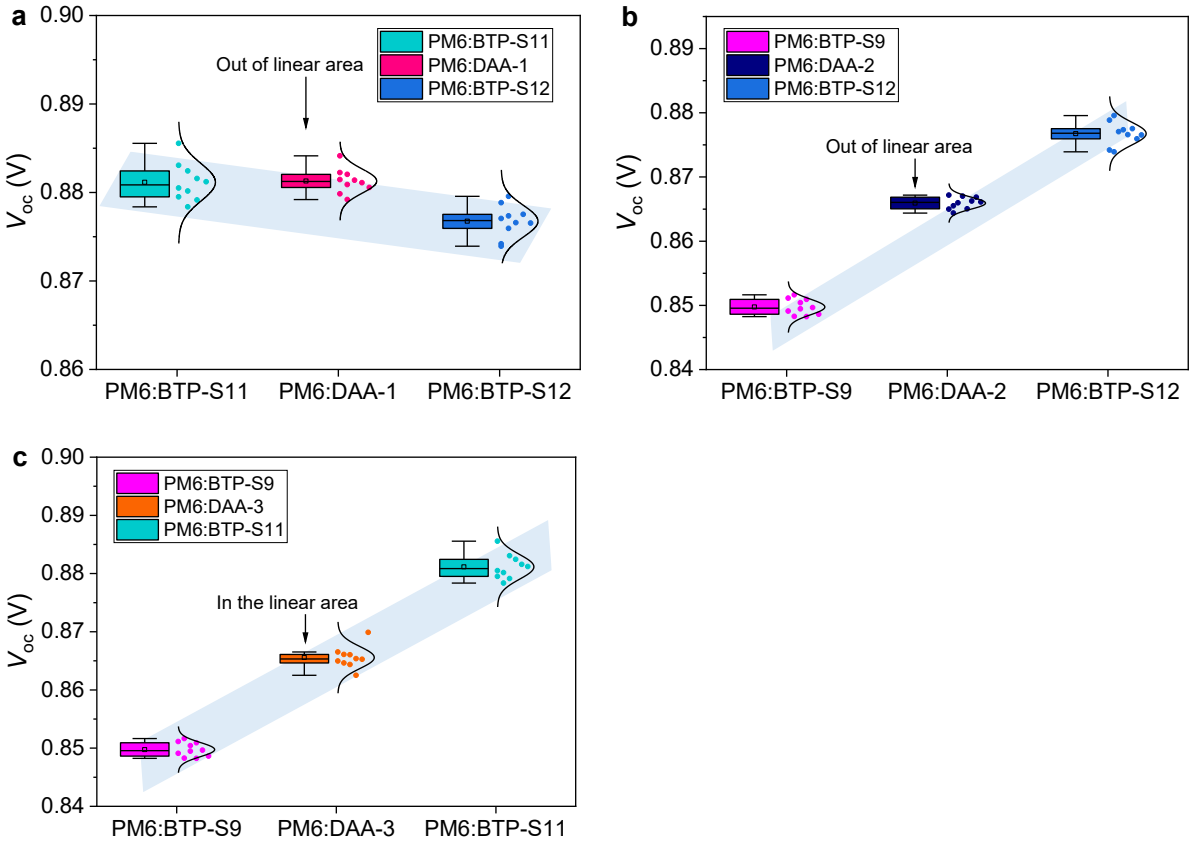

Fig. S11 (a) Voltage comparison among PM6:BTP-S11, PM6:DAA-1 and PM6:BTP-S12-based OPVs. (b) Voltage comparison among PM6:BTP-S9, PM6:DAA-2 and PM6:BTP-S12-based OPVs. (c) Voltage comparison among PM6:BTP-S9, PM6:DAA-3 and PM6:BTP-S11-based OPVs.

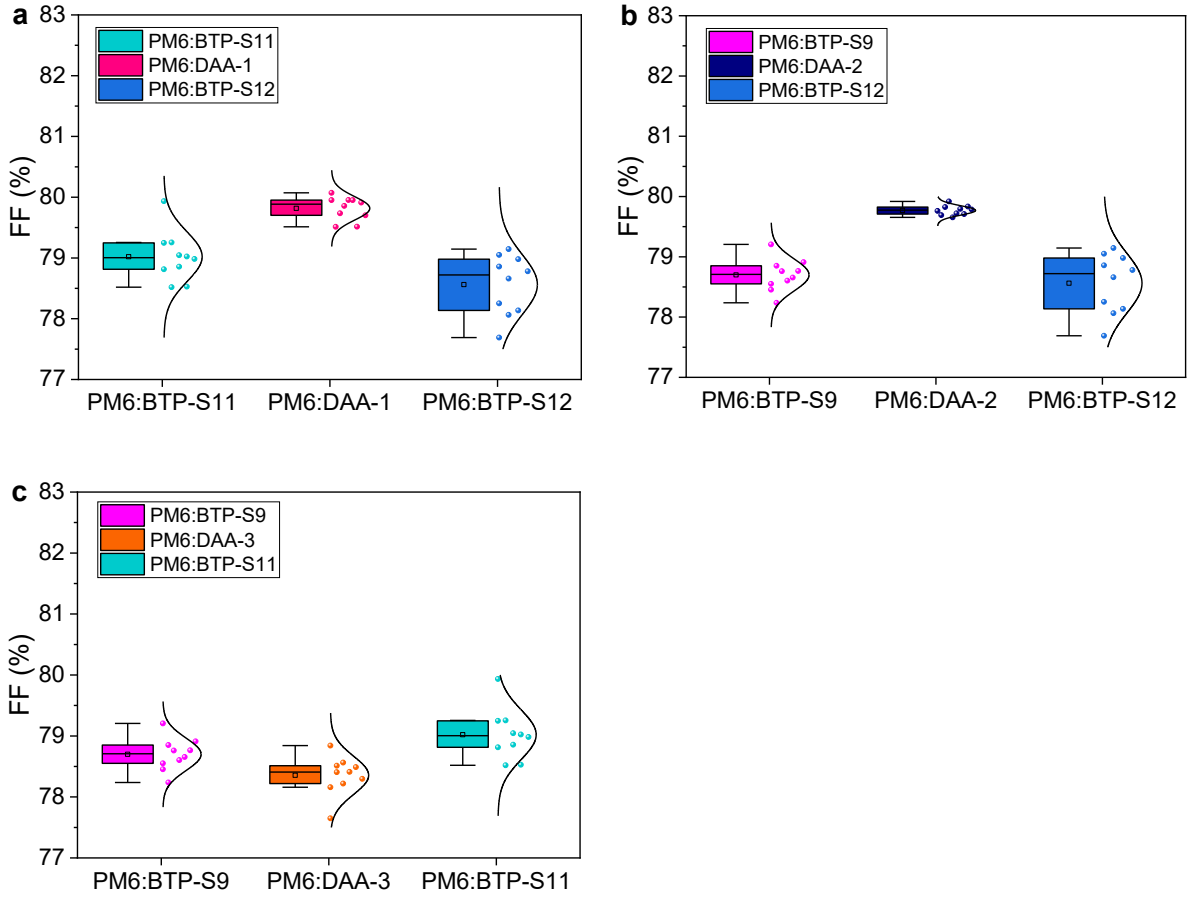

Fig. S12 (a) FF comparison among PM6:BTP-S11, PM6:DAA-1 and PM6:BTP-S12-based OPVs. (b) FF comparison among PM6:BTP-S9, PM6:DAA-2 and PM6:BTP-S12-based OPVs. (c) FF comparison among PM6:BTP-S9, PM6:DAA-3 and PM6:BTP-S11-based OPVs.

福建省计量科学研究院
FUJIAN METROLOGY INSTITUTE
（国家光伏产业计量测试中心）
National PV Industry Measurement and Testing Center

检 测 报 告
Test Report

报告编号：22Q3-00030
Report No.

客户名称 Name of Customer	Zhejiang University
联络信息 Contact Information	Zhejiang University, No. 38 Yugu Road, Hangzhou, Zhejiang Province, P. R. China
物品名称 Name of items	Organic Solar Cells
型号/规格 Type /Specification	1.5cm × 1.5cm
物品编号 Items No	PM6:BTP-S11:BTP-S12
制造厂商 Manufacturer	Department of Polymer Science & Engineering, Zhejiang University
物品接收日期 Items Receipt Date	2022-01-29
检测日期 Test Date	2022-01-29

批准人 Approved by 黎健生
核验员 Checked by 何翔
检测员 Test by 陈彩云

发布日期 Date of Report 2022 年 Year 02 月 month 08 日 Day

扫一扫 查真伪

本院/本中心地址：福州市屏东路 9-3 号 Address：9-3 Pingdong Road.Fuzhou.China
电话：0591-87845050 Telephone
传真：0591-87808417 Fax
邮编：350003 Post Code
网址：www.fjjl.net Web Site
咨询电话：0591-87845050 Inquire line
投诉电话：0591-87823025 Complaint Tel

未经本院/本中心书面批准，部分复制采用本报告内容无效。
Partly using this Report will not be admitted unless allowed by FMI/ Center.

第 1 页/共 7 页 Page of Pages

Fig. S13 The copy of certified report from National PV Industry Measurement and Testing Center (NPVIM) for ternary device (PM6:DAA-4 based ternary OPV).

福建省计量科学研究院
FUJIAN METROLOGY INSTITUTE
（国家光伏产业计量测试中心）
National PV Industry Measurement and Testing Center

报告编号：22Q3-00030
Report No.

1. 检测机构说明：
Testing institutions that

本院为国家法定计量检定机构，国家光伏产业计量测试中心依托本院检测技术开展检测。本院/本中心质量管理体系符合 GB/T 27025（ISO/IEC 17025，IDT）标准要求。

The institute is a national legal metrological institution. National PV Industry Measurement and Testing Center carrys out testing relying on the institute's testing technology. The Center's quality management system meets the requirements of GB/T 27025（ISO/IEC 17025，IDT）standard.

2. 本次检测所依据的检测方法（代号及名称）：
Reference documents from the test (code,name)

IEC 60904-1-2020 光伏器件-第一部分：光伏电流-电压特性的测量;IEC 60904-8:2014 光伏器件-第 8 部分光伏器件的光谱响应度测量

3. 本次检测所使用的主要测量仪器：
Measurement standards used in this test

仪器名称 Name	仪器编号 Number	测量范围 Measuring Range	不确定度/或准确度等级/或最大允许误差 Uncertainty or Accuracy Class or Maximum Permissible Error	溯源机构名称/证书编号 Name of traceability institution/Certificate No.	有效期限 Due date
系统源表（电子负载）	4082810	100 nA～3 A；(0.1～40) V	U_{rel}=0.005% (k=2)	上海市计量院 2021F11-10-3083069001	2022-03-10
太阳模拟器	2015-006	(300～1200) nm；(800～1200) W/m^2	光谱匹配度：(300～310) nm：U_{rel}=7.4% (k=2);(310～400) nm：U_{rel}=6.4% (k=2);(400～1200) nm：U_{rel}=5.5% (k=2);辐照度比：U_{rel}=1.2% (k=2)	福建计量院 21Q2-00682	2022-06-28
WPVS 单晶硅标准电池	015-2014	(300～1200) nm	U_{rel}=1.3% (k=2)	中国计量院 GXgf2021-10725	2023-04-05
Si 光电探测器	Si-2	(200~1100)nm	(300～450) nm U_{rel}=1.8%～1.3% (k=2) ; (450～1000) nm U_{rel}=1.2%～1.7% (k=2)	中国计量院 GXgf2021-10903	2023-03-24
数字温度计	15-B	(15～65)℃	U=0.1% (k=2)	福建计量院 21B2-08012	2022-06-22

4. 检测地点及环境条件：
Location and environmental condition for the test

地点：Room 108, Building 4, MinHou Scientific Research Base
Location

温度：24.5 ℃ Temperature　　相对湿度：48 % Relative Humidity　　其它：/ Others

5. 备注：/
Note

本报告提供的结果仅对本次被检的物品有效。
The data are valid only for the instrument(s) under testing.

检测报告续页专用
Continued page of test report

Fig. S13-continued The copy of certified report from National PV Industry Measurement and Testing Center (NPVIM) for ternary device (PM6:DAA-4 based ternary OPV).

福建省计量科学研究院
FUJIAN METROLOGY INSTITUTE
（国家光伏产业计量测试中心）
National PV Industry Measurement and Testing Center

报告编号：22Q3-00030
Report No.

检测结果/说明：
Results of Test and additional explanation.

1 Standard Test Condition (STC)： Total Irradiance：1000 W/m^2
Temperature：25.0 ℃
Spectral Distribution：AM1.5G

2 Measurement Data and I-V/P-V Curves under STC

Forward Scan

I_{sc} (mA)	V_{oc} (V)	I_{MPP} (mA)	V_{MPP} (V)	P_{MPP} (mW)	*FF* (%)	η (%)
1.231	0.8848	1.142	0.7578	0.8654	79.45	18.51

Reverse Scan

I_{sc} (mA)	V_{oc} (V)	I_{MPP} (mA)	V_{MPP} (V)	P_{MPP} (mW)	*FF* (%)	η (%)
1.231	0.8841	1.142	0.7578	0.8654	79.52	18.51

Mismatch factor: 0.9918

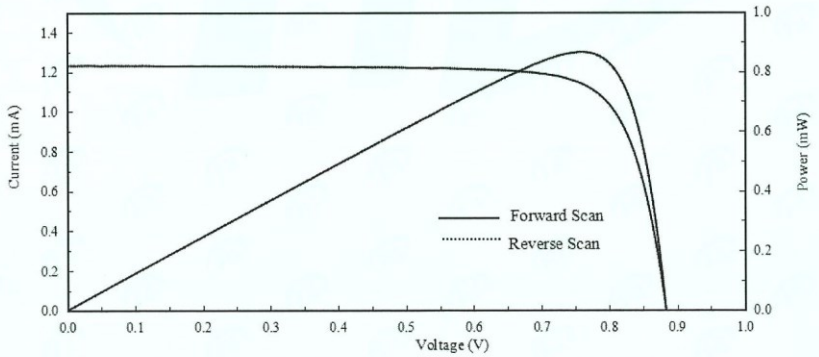

Figure 1. I-V and P-V characteristic curves of the measured sample under STC

检测报告续页专用
Continued page of test report

第 3 页/共 7 页
Page of Pages

Fig. S13-continued The copy of certified report from National PV Industry Measurement and Testing Center (NPVIM) for ternary device (PM6:DAA-4 based ternary OPV).

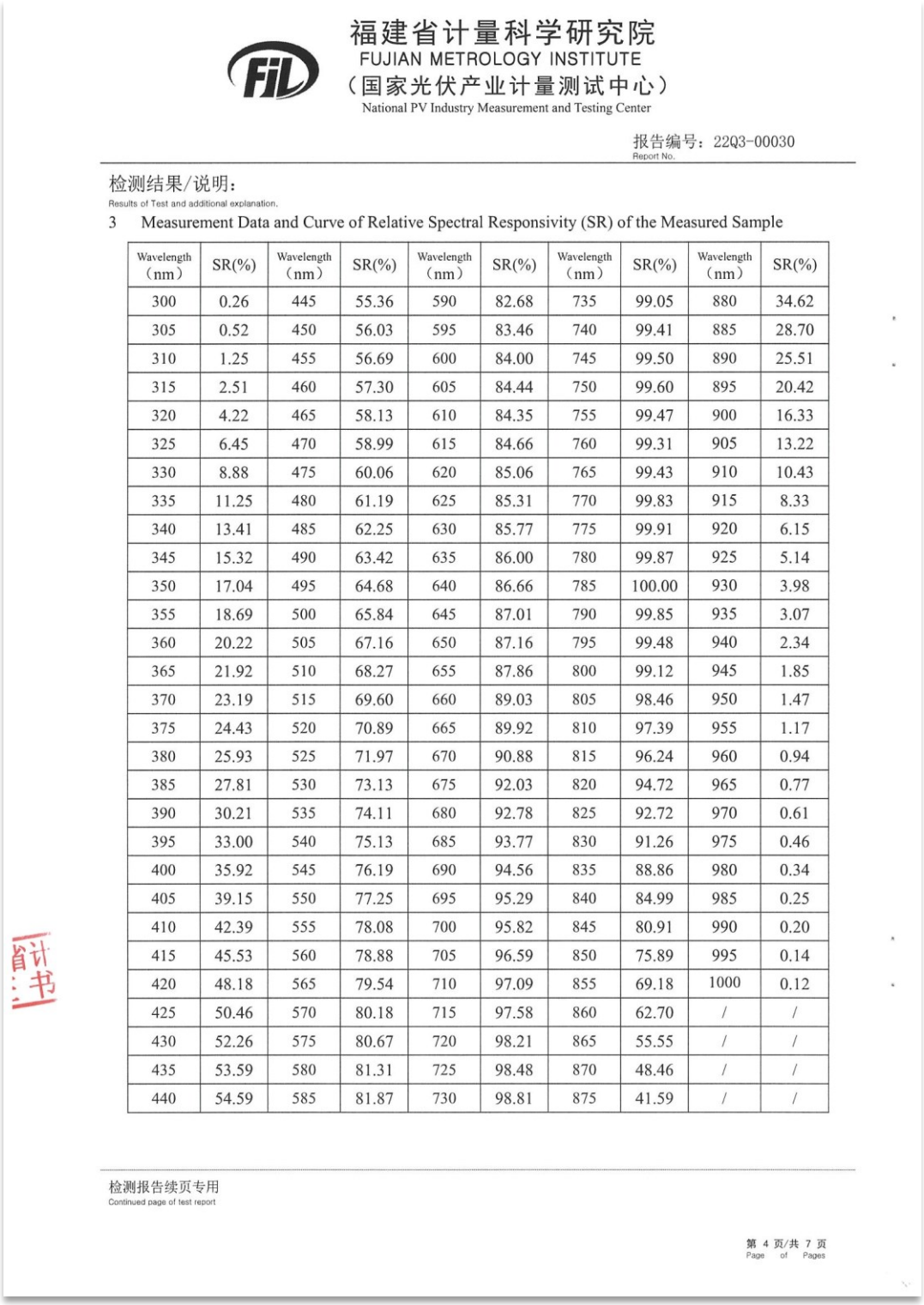

福建省计量科学研究院
FUJIAN METROLOGY INSTITUTE
（国家光伏产业计量测试中心）
National PV Industry Measurement and Testing Center

报告编号：22Q3-00030
Report No.

检测结果/说明：
Results of Test and additional explanation.

3 Measurement Data and Curve of Relative Spectral Responsivity (SR) of the Measured Sample

Wavelength (nm)	SR(%)	Wavelength (nm)	SR(%)	Wavelength (nm)	SR(%)	Wavelength (nm)	SR(%)	Wavelength (nm)	SR(%)
300	0.26	445	55.36	590	82.68	735	99.05	880	34.62
305	0.52	450	56.03	595	83.46	740	99.41	885	28.70
310	1.25	455	56.69	600	84.00	745	99.50	890	25.51
315	2.51	460	57.30	605	84.44	750	99.60	895	20.42
320	4.22	465	58.13	610	84.35	755	99.47	900	16.33
325	6.45	470	58.99	615	84.66	760	99.31	905	13.22
330	8.88	475	60.06	620	85.06	765	99.43	910	10.43
335	11.25	480	61.19	625	85.31	770	99.83	915	8.33
340	13.41	485	62.25	630	85.77	775	99.91	920	6.15
345	15.32	490	63.42	635	86.00	780	99.87	925	5.14
350	17.04	495	64.68	640	86.66	785	100.00	930	3.98
355	18.69	500	65.84	645	87.01	790	99.85	935	3.07
360	20.22	505	67.16	650	87.16	795	99.48	940	2.34
365	21.92	510	68.27	655	87.86	800	99.12	945	1.85
370	23.19	515	69.60	660	89.03	805	98.46	950	1.47
375	24.43	520	70.89	665	89.92	810	97.39	955	1.17
380	25.93	525	71.97	670	90.88	815	96.24	960	0.94
385	27.81	530	73.13	675	92.03	820	94.72	965	0.77
390	30.21	535	74.11	680	92.78	825	92.72	970	0.61
395	33.00	540	75.13	685	93.77	830	91.26	975	0.46
400	35.92	545	76.19	690	94.56	835	88.86	980	0.34
405	39.15	550	77.25	695	95.29	840	84.99	985	0.25
410	42.39	555	78.08	700	95.82	845	80.91	990	0.20
415	45.53	560	78.88	705	96.59	850	75.89	995	0.14
420	48.18	565	79.54	710	97.09	855	69.18	1000	0.12
425	50.46	570	80.18	715	97.58	860	62.70	/	/
430	52.26	575	80.67	720	98.21	865	55.55	/	/
435	53.59	580	81.31	725	98.48	870	48.46	/	/
440	54.59	585	81.87	730	98.81	875	41.59	/	/

检测报告续页专用
Continued page of test report

第 4 页/共 7 页
Page of Pages

Fig. S13-continued The copy of certified report from National PV Industry Measurement and Testing Center (NPVIM) for ternary device (PM6:DAA-4 based ternary OPV).

福建省计量科学研究院
FUJIAN METROLOGY INSTITUTE
（国家光伏产业计量测试中心）
National PV Industry Measurement and Testing Center

报告编号：22Q3-00030
Report No.

检测结果/说明：
Results of Test and additional explanation.

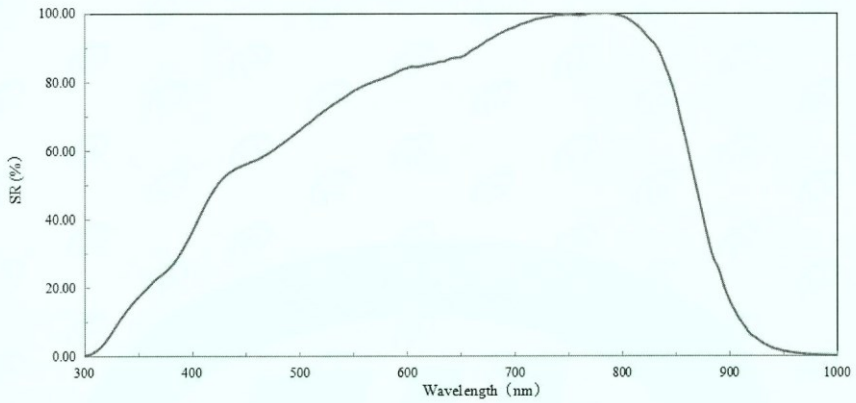

Figure 2. Relative spectral responsivity curve of the measured sample

4 Pictures of the Measured Sample

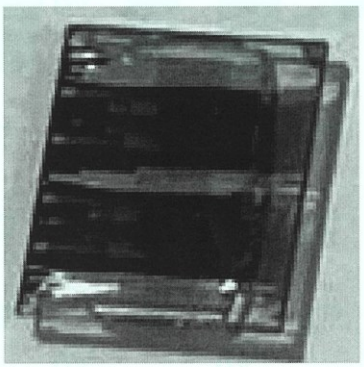

Figure 3. Obverse side of the measured sample

检测报告续页专用
Continued page of test report

第 5 页/共 7 页
Page of Pages

Fig. S13-continued The copy of certified report from National PV Industry Measurement and Testing Center (NPVIM) for ternary device (PM6:DAA-4 based ternary OPV).

福建省计量科学研究院
FUJIAN METROLOGY INSTITUTE
（国家光伏产业计量测试中心）
National PV Industry Measurement and Testing Center

报告编号：22Q3-00030
Report No.

检测结果/说明：
Results of Test and additional explanation.

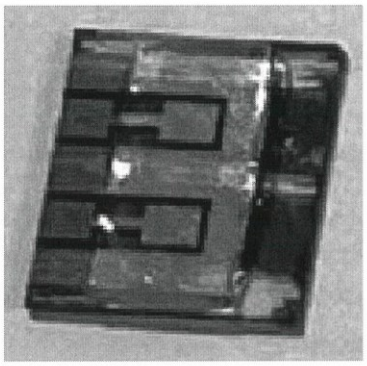

Figure 4. Reverse side of the measured sample

Uncertainty of measurement results:

Short-Circuit Current: U_{rel}=1.4% (k=2); Open-Circuit Voltage: U_{rel}=1.0% (k=2);

Maximum Power: U_{rel}=2.2% (k=2); Efficiency: U_{rel}=2.2% (k=2); Fill Factor: U_{rel}=3.2% (k=2).

Relative Spectral Responsivity:

(300~400) nm: U_{rel} = 2.2% (k=2);

(400~1000) nm: U_{rel} = 1.8% (k=2).

说明：The effective area of the measured sample was 0.04675 cm^2.
Explanation

Testing method (code and name) for this test
IEC 60904-1: 2020 Photovoltaic devices- Part 1: Measurement of photovoltaic current-voltage characteristics
IEC 60904-8: 2014 Photovoltaic devices- Part 8: Measurement of spectral responsivity of a photovoltaic (PV) device

检测报告续页专用
Continued page of test report

第 6 页/共 7 页
Page of Pages

Fig. S13-continued The copy of certified report from National PV Industry Measurement and Testing Center (NPVIM) for ternary device (PM6:DAA-4 based ternary OPV).

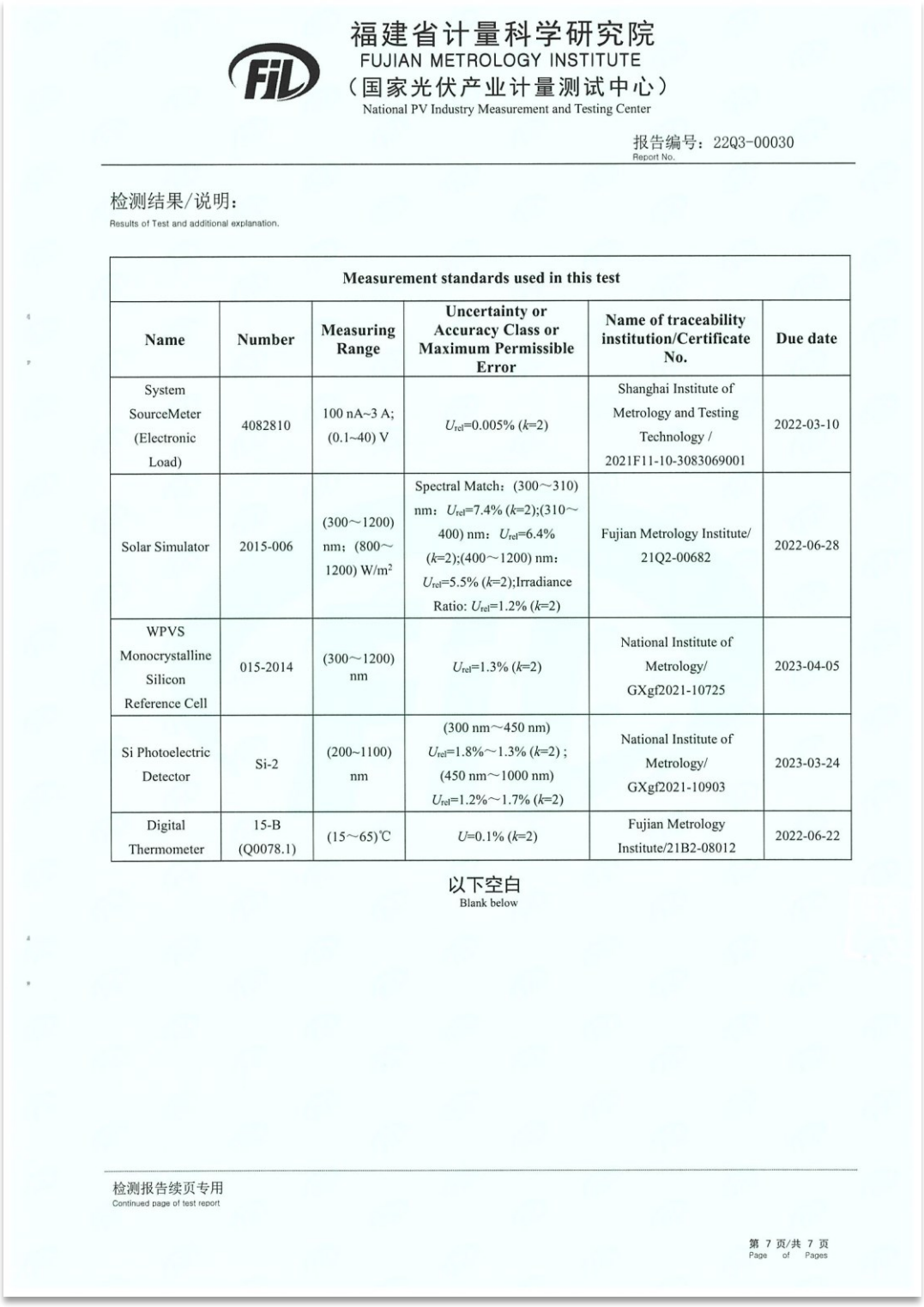

福建省计量科学研究院
FUJIAN METROLOGY INSTITUTE
（国家光伏产业计量测试中心）
National PV Industry Measurement and Testing Center

报告编号：22Q3-00030
Report No.

检测结果/说明：
Results of Test and additional explanation.

Measurement standards used in this test					
Name	**Number**	**Measuring Range**	**Uncertainty or Accuracy Class or Maximum Permissible Error**	**Name of traceability institution/Certificate No.**	**Due date**
System SourceMeter (Electronic Load)	4082810	100 nA~3 A; (0.1~40) V	U_{rel}=0.005% (k=2)	Shanghai Institute of Metrology and Testing Technology / 2021F11-10-3083069001	2022-03-10
Solar Simulator	2015-006	(300～1200) nm；(800～1200) W/m^2	Spectral Match：(300～310) nm：U_{rel}=7.4% (k=2);(310～400) nm：U_{rel}=6.4% (k=2);(400～1200) nm：U_{rel}=5.5% (k=2);Irradiance Ratio: U_{rel}=1.2% (k=2)	Fujian Metrology Institute/ 21Q2-00682	2022-06-28
WPVS Monocrystalline Silicon Reference Cell	015-2014	(300～1200) nm	U_{rel}=1.3% (k=2)	National Institute of Metrology/ GXgf2021-10725	2023-04-05
Si Photoelectric Detector	Si-2	(200~1100) nm	(300 nm～450 nm) U_{rel}=1.8%～1.3% (k=2)；(450 nm～1000 nm) U_{rel}=1.2%～1.7% (k=2)	National Institute of Metrology/ GXgf2021-10903	2023-03-24
Digital Thermometer	15-B (Q0078.1)	(15～65)℃	U=0.1% (k=2)	Fujian Metrology Institute/21B2-08012	2022-06-22

以下空白
Blank below

检测报告续页专用
Continued page of test report

第 7 页/共 7 页
Page of Pages

Fig. S13-continued The copy of certified report from National PV Industry Measurement and Testing Center (NPVIM) for ternary device (PM6:DAA-4 based ternary OPV).

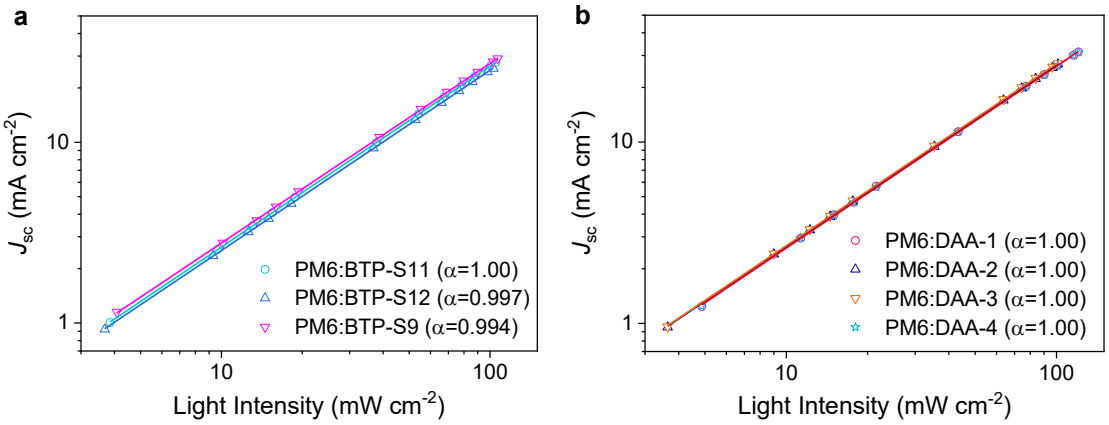

Fig. S14 (a) The dependence of J_{sc} on light intensity (P_{light}) of relevant binary OPVs. (b) The dependence of J_{sc} on P_{light} of relevant ternary OPVs.

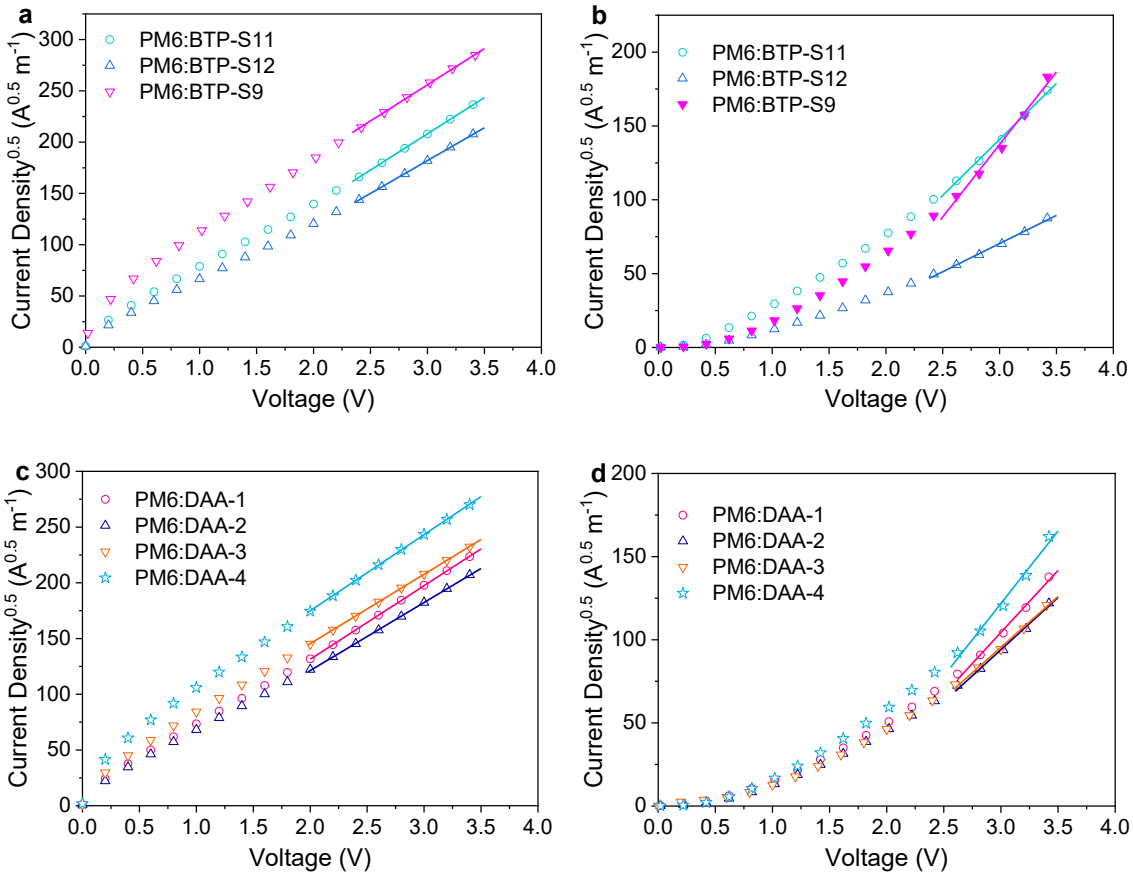

Fig. S15 (a) $J^{0.5}$-V curves of the hole-only devices based on PM6:BTP-S11, PM6:BTP-S12 and PM6:BTP-S9 blends (Device: ITO/PEDOT:PSS/Active layer/MoO_3/Ag). (b) $J^{0.5}$-V curves of the electron-only devices based on PM6:BTP-S11, PM6:BTP-S12 and PM6:BTP-S9 blends (Device: ITO/ZnO/Active layer/Bis-FIMG/Ag). (c) $J^{0.5}$-V curves of the hole-only devices based on PM6:DAA-1, PM6:DAA-2, PM6:DAA-3 and PM6:DAA-4 blends (Device: ITO/PEDOT:PSS/Active layer/MoO_3/Ag). (d) $J^{0.5}$-V curves of the electron-only devices based on PM6:DAA-1, PM6:DAA-2, PM6:DAA-3 and PM6:DAA-4 blends (Device: ITO/ZnO/Active layer/Bis-FIMG/Ag).

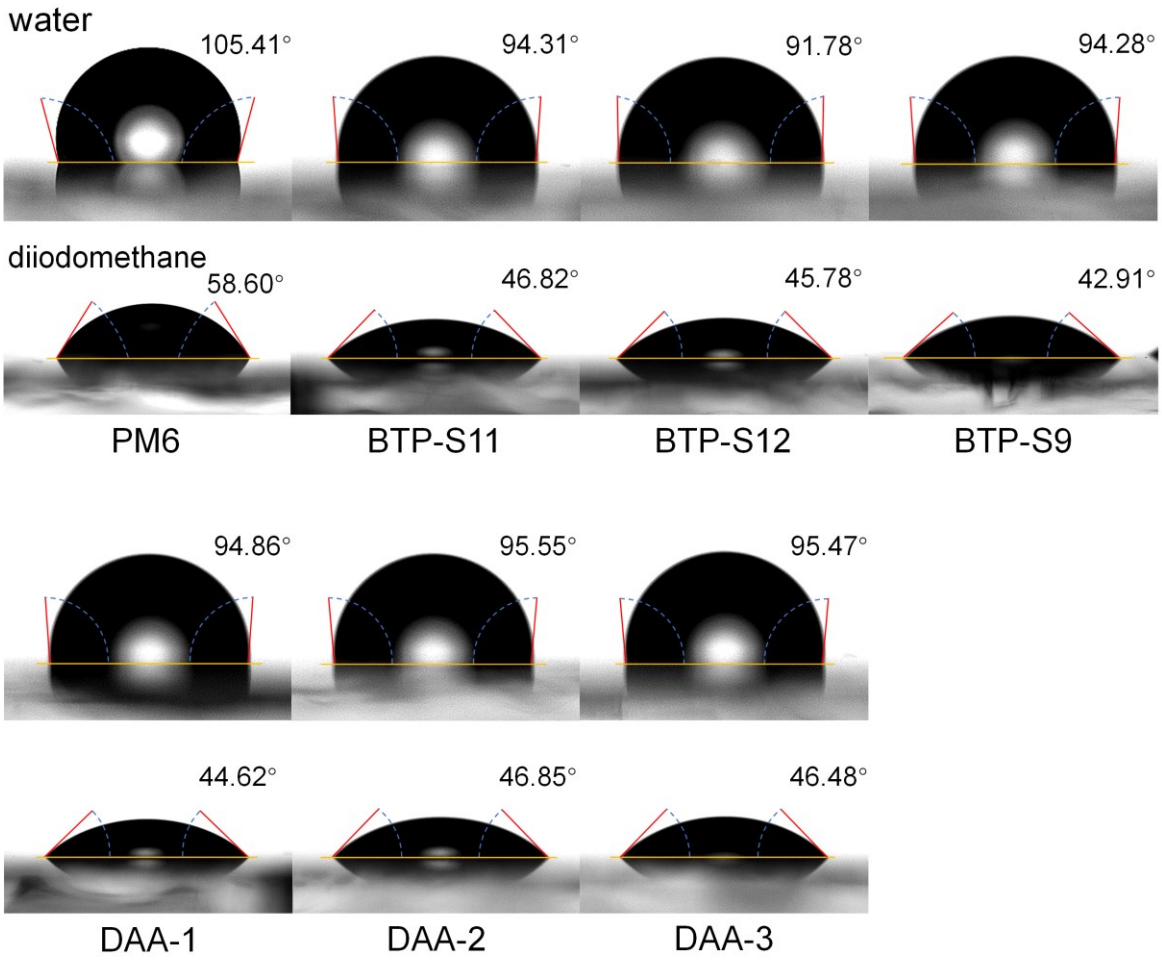

Fig. S16 Contact angle images of PM6, BTP-S11, BTP-S12, BTP-S9, DAA-1, DAA-2 and DAA-3 films with water and diiodomethane droplets on top. Relevant miscibility parameters are summarized in **Table S3**.

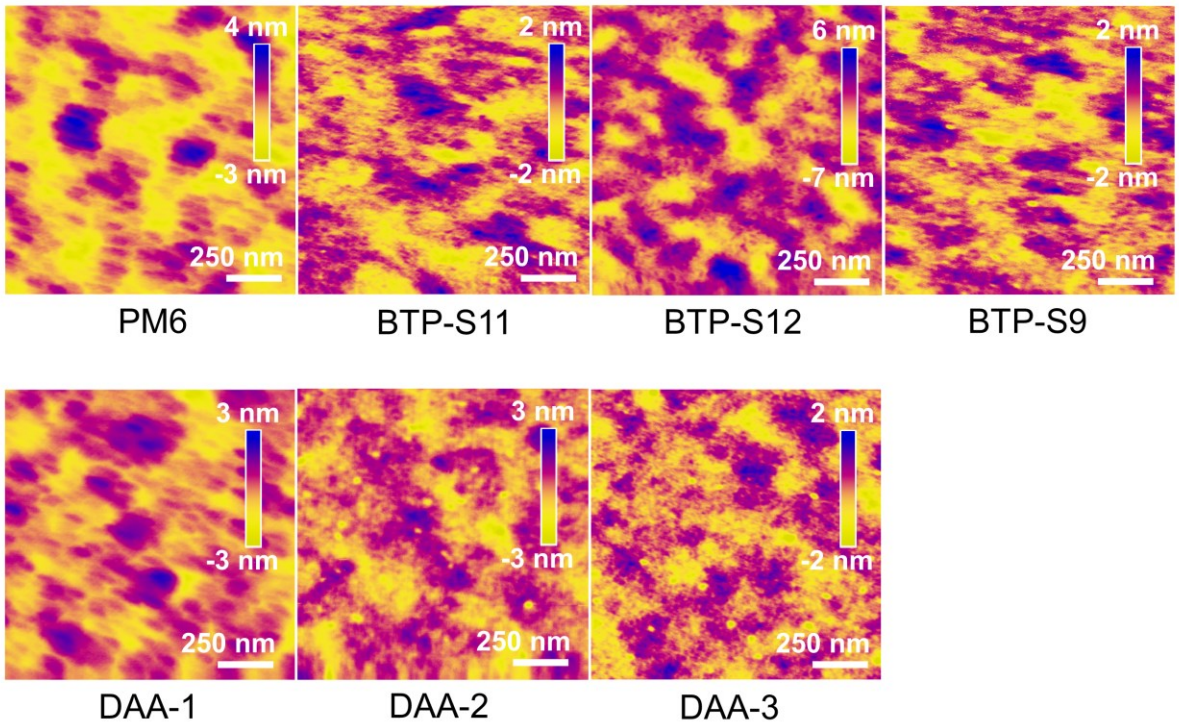

Fig. S17 AFM height images of PM6, BTP-S11, BTP-S12, BTP-S9, DAA-1, DAA-2 and DAA-3 films. Relevant roughness data are listed in **Table S3**.

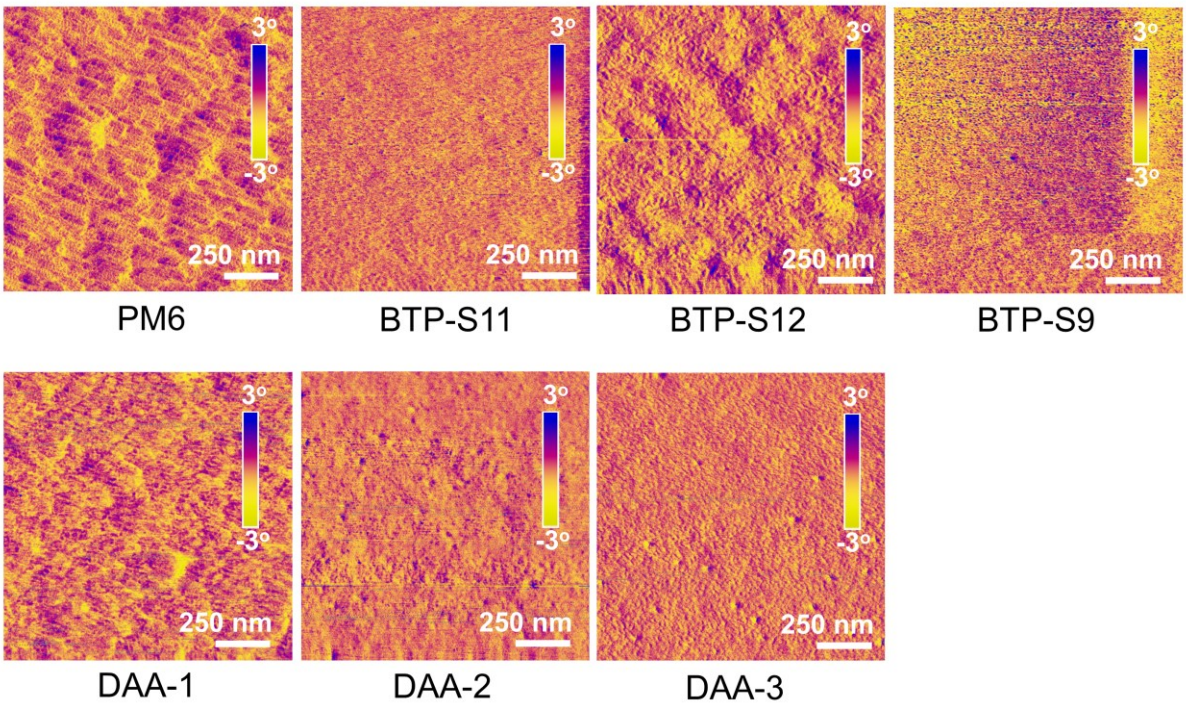

Fig. S18 AFM phase images of PM6, BTP-S11, BTP-S12, BTP-S9, DAA-1, DAA-2 and DAA-3 films.

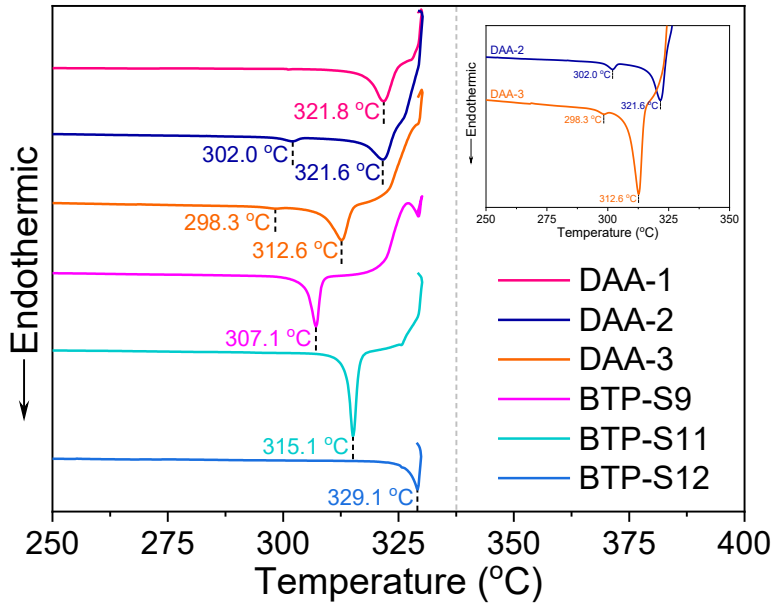

Fig. S19 DSC curves of BTP-S9, BTP-S11, BTP-S12, DAA-1, DAA-2 and DAA-3.

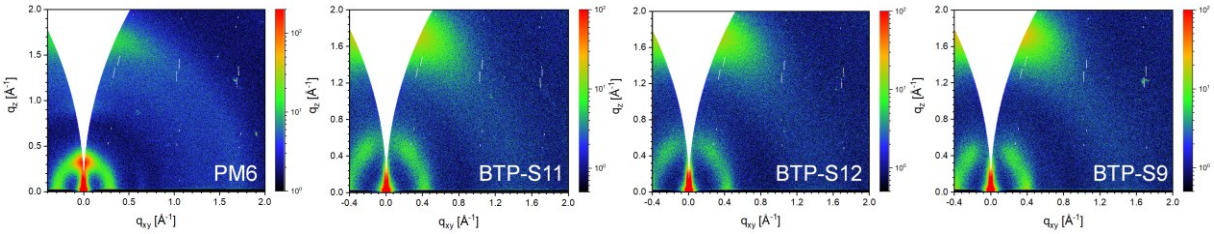

Fig. S20 2D GIWAXS images for PM6, BTP-S11, BTP-S12 and BTP-S9 neat films.

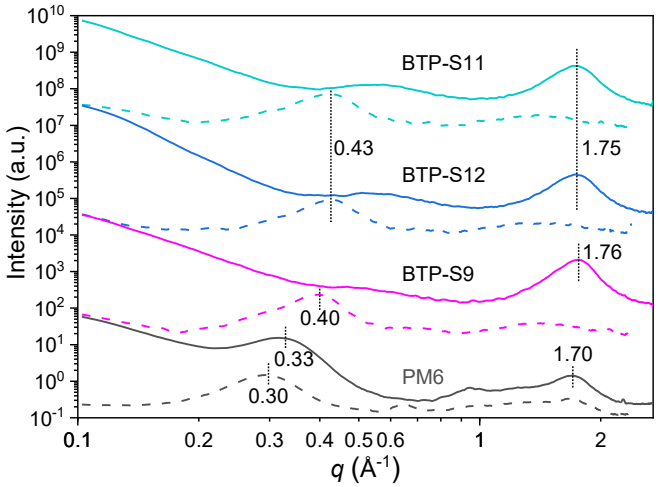

Fig. S21 1D intensity profiles of PM6, BTP-S11, BTP-S12 and BTP-S9 neat films in the out-of-plane (OOP, solid lines) and in-plane (IP, dash lines) directions.

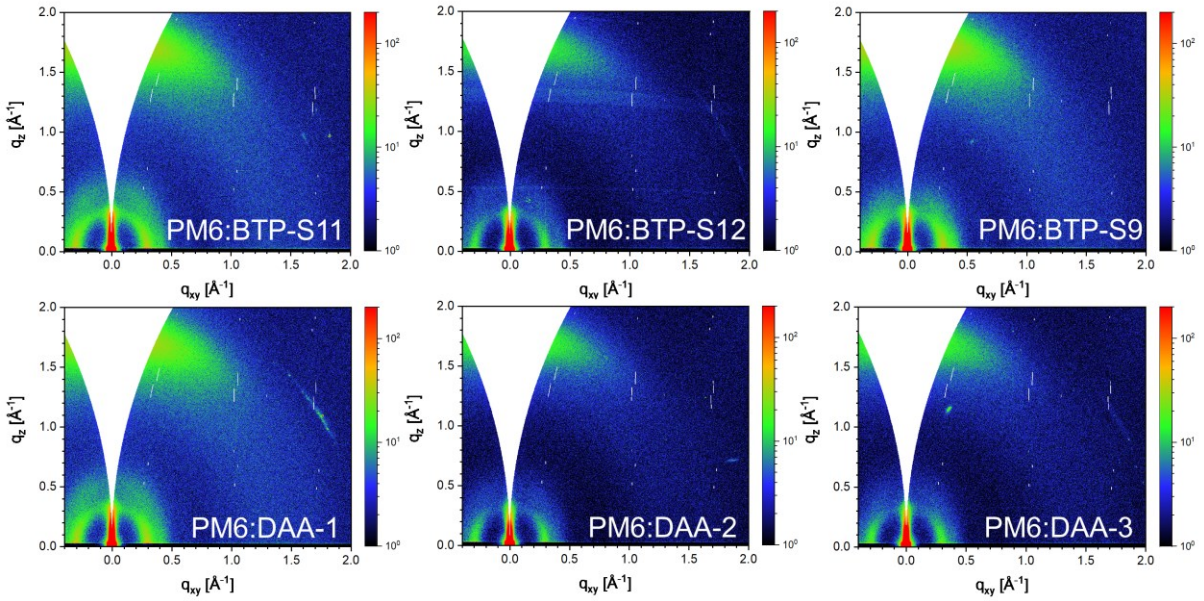

Fig. S22 2D GIWAXS images for PM6:BTP-S11, PM6:BTP-S12, PM6:BTP-S9, PM6:DAA-1, PM6:DAA-2 and PM6:DAA-3 blend films.

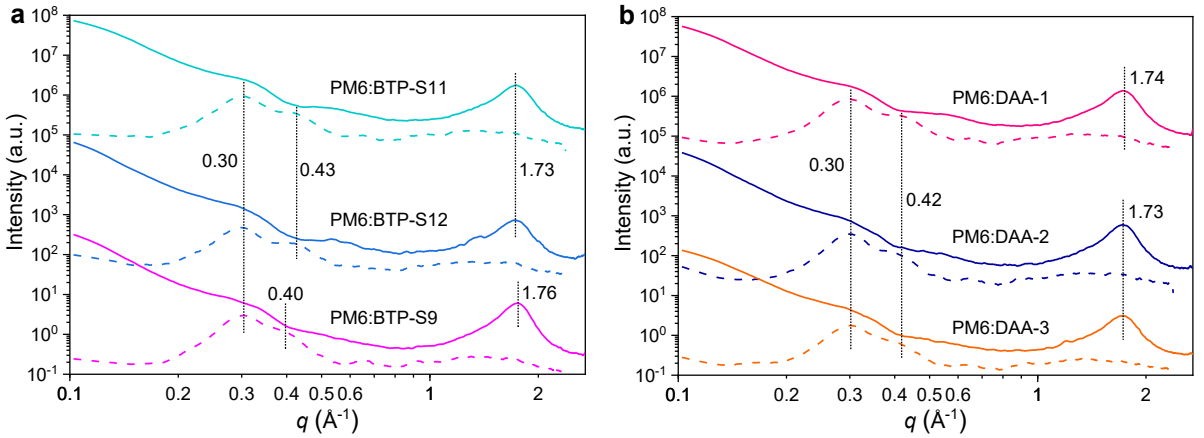

Fig. S23 (a) 1D intensity profiles of PM6:BTP-S11, PM6:BTP-S12 and PM6:BTP-S9 blends in the OOP (solid lines) and IP (dash lines) directions. (b) 1D intensity profiles of PM6:DAA-1, PM6:DAA-2 and PM6:DAA-3 blends in the OOP (solid lines) and IP (dash lines) directions.

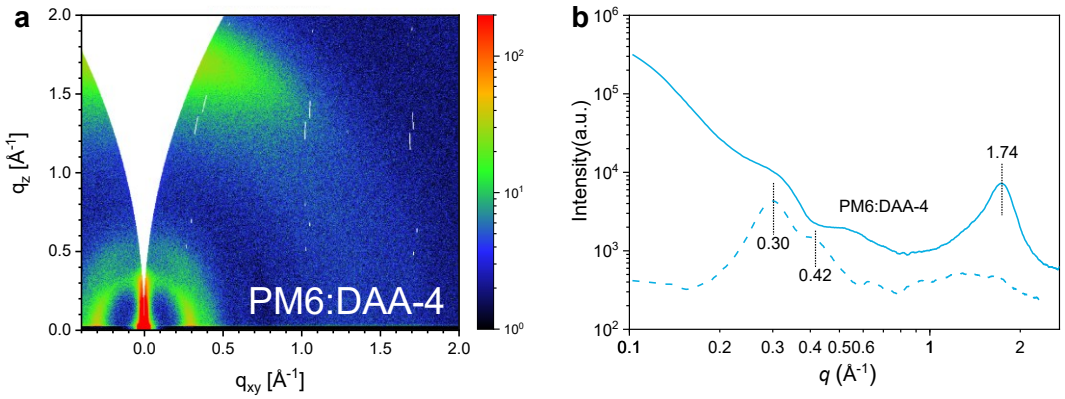

Fig. S24 (a) 2D GIWAXS image of PM6:DAA-4 blend. (b) 1D intensity profiles of PM6:DAA-4 blend in the OOP (solid line) and IP (dash line) directions.

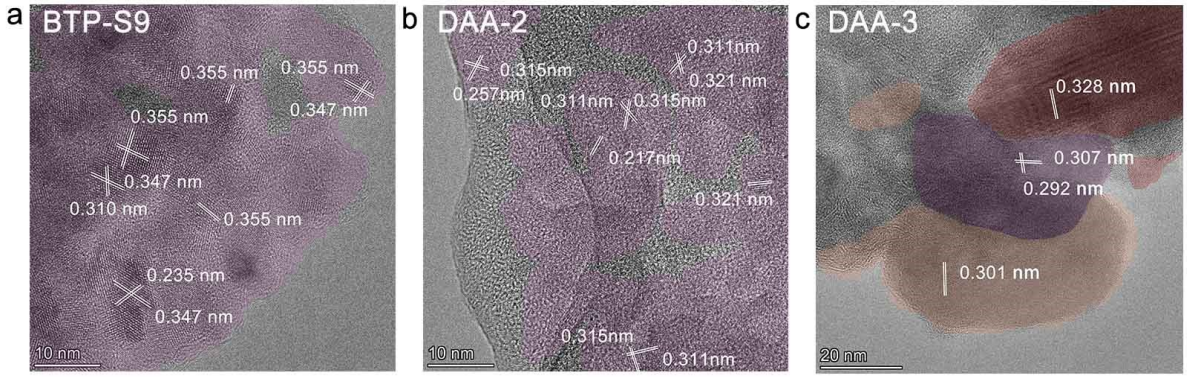

Fig. S25 (a) HR-TEM image of BTP-S9 film. (b) HR-TEM image of DAA-2 film. (c) HR-TEM image of DAA-3 film.

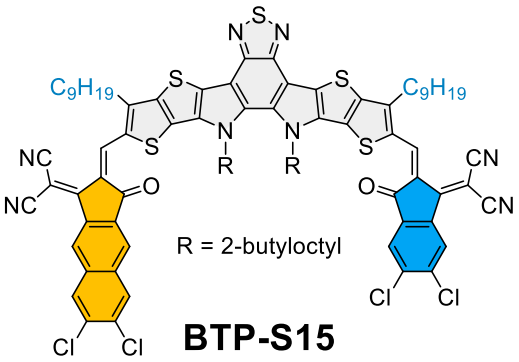

Fig. S26 Chemical structure of BTP-S15.

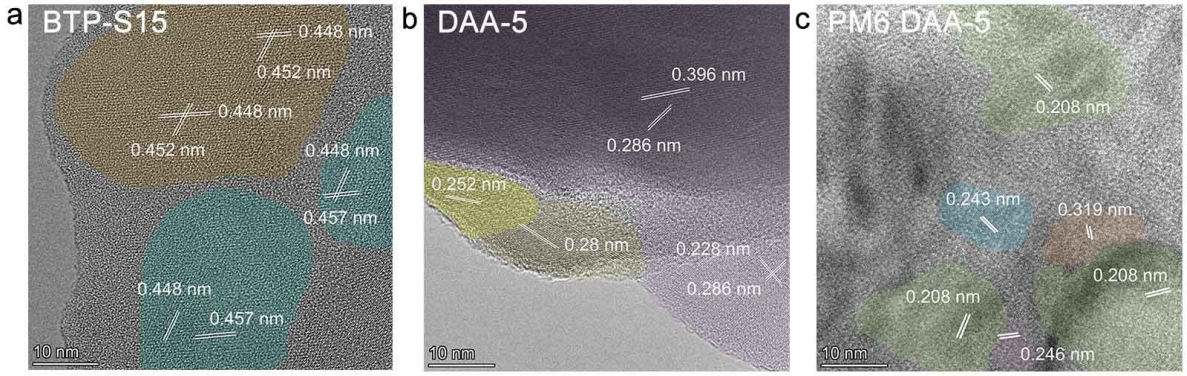

Fig. S27 (a) HR-TEM image of BTP-S15 film. (b) HR-TEM image of DAA-5 film (DAA-5: BTP-S9:BTP-S15 = 1:1). (c) HR-TEM image of PM6:DAA-5 film.

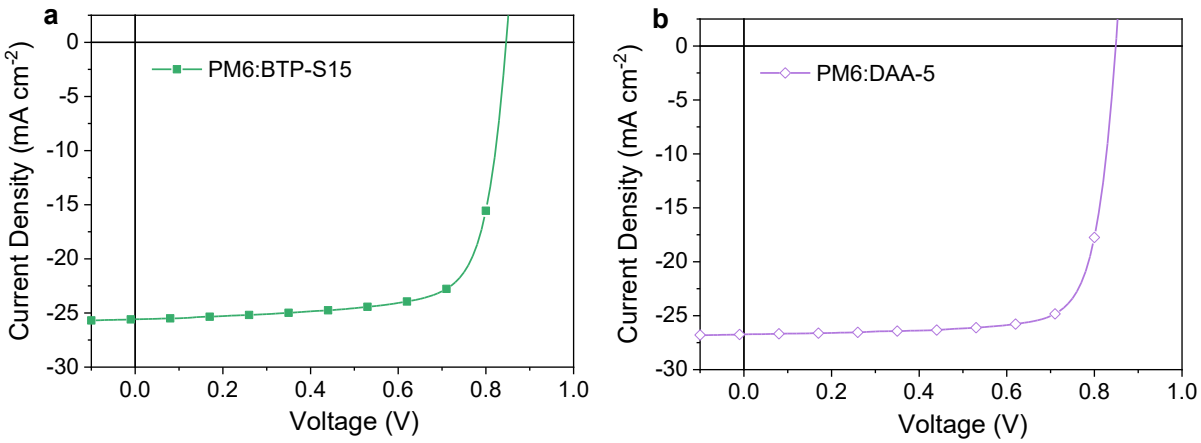

Fig. S28 (a) *J*-*V* curve of PM6:BTP-S15-based OPV (V_{oc}: 0.846 V; J_{sc}: 25.6 mA cm^{-2}; FF: 74.9%; PCE: 16.1%). (b) *J*-*V* curve of PM6:DAA-5-based OPV (DAA-5: BTP-S9:BTP-S15 = 1:1; V_{oc}: 0.849 V; J_{sc}: 26.7 mA cm^{-2}; FF: 78.1%; PCE: 17.7%).

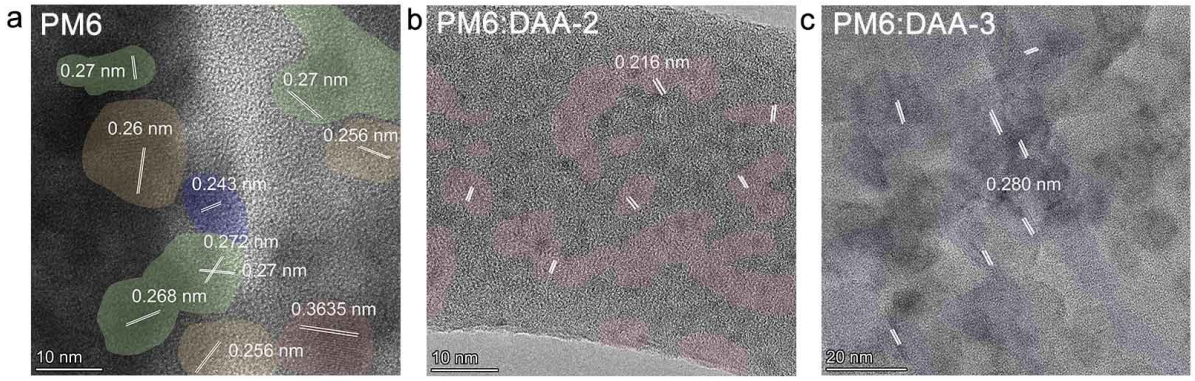

Fig. S29 (a) HR-TEM image of PM6 film. (b) HR-TEM image of PM6:DAA-2 film. (c) HR-TEM image of PM6:DAA-3 film.

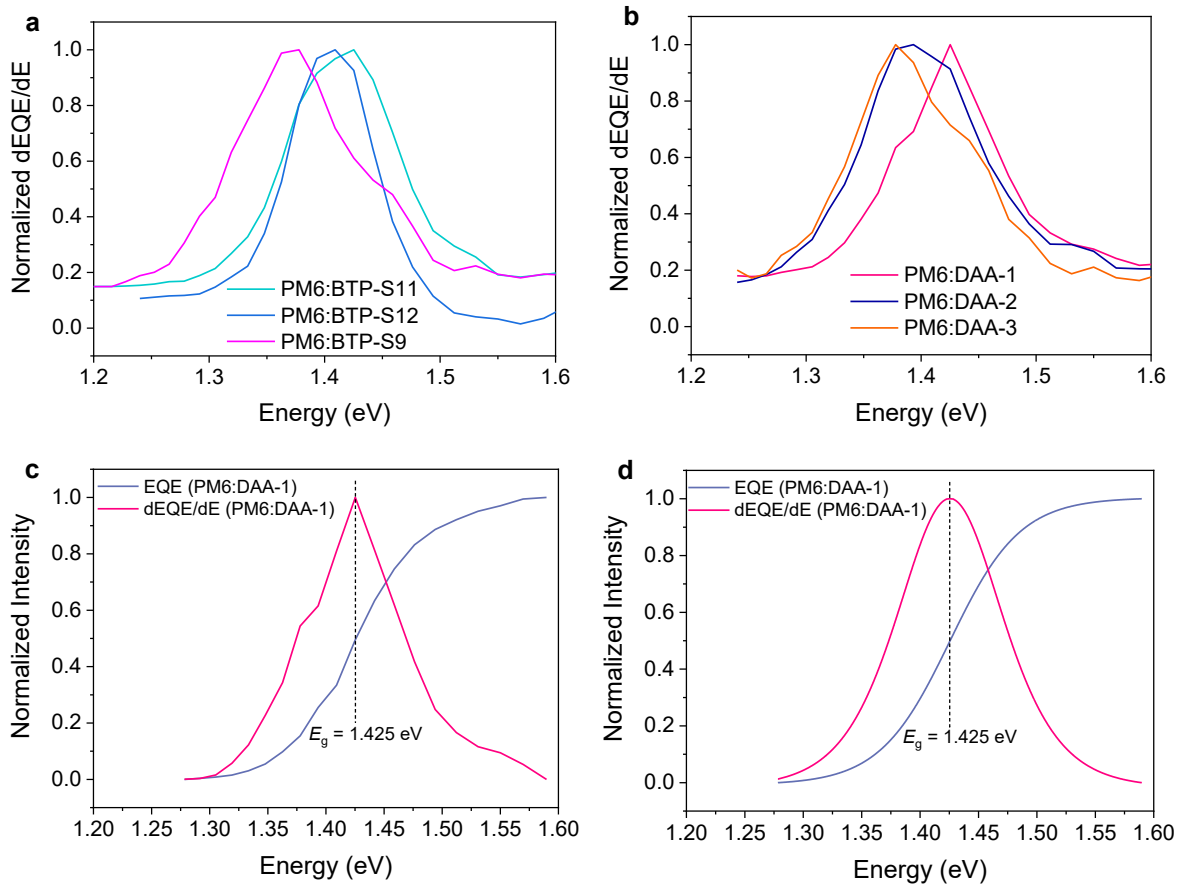

Fig. S30 (a) Bandgap distributions for OPVs based on PM6:BTP-S11, PM6:BTP-S12 and PM6:BTP-S9 blends. (b) Bandgap distributions for OPVs based on PM6:DAA-1, PM6:DAA-2 and PM6:DAA-3 blends. (c) Determination of bandgap for PM6:DAA-1 based device. (d) Determination of bandgap for PM6:DAA-1 based device with the smoother EQE curve.

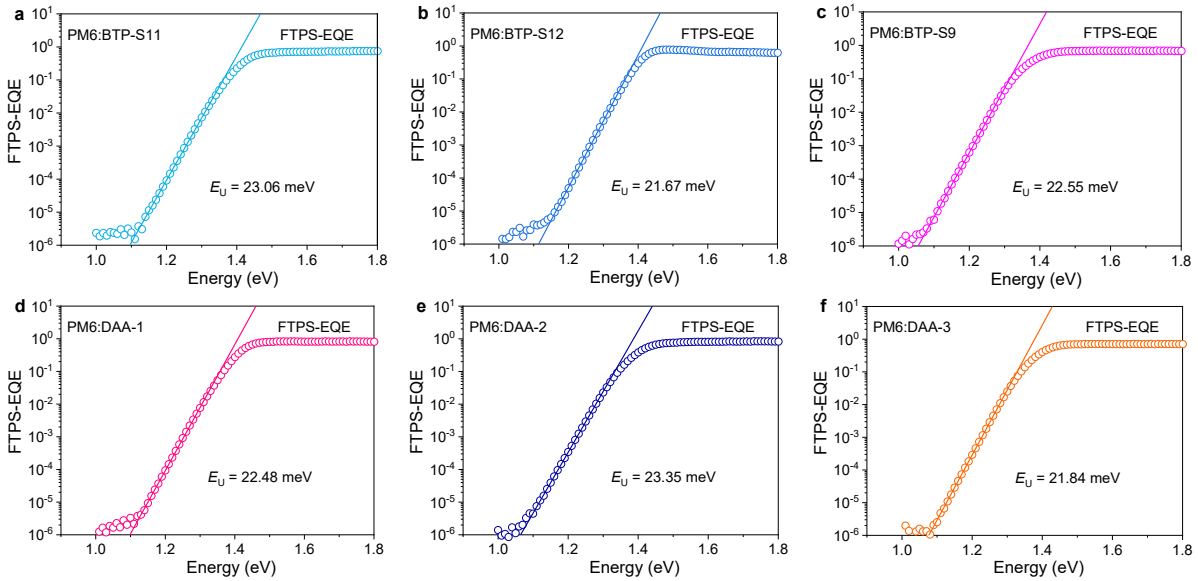

Fig. S31 (a-f) Determination of Urbach energy (E_U) via exponential fitting of FTPS-EQE curves for PM6:BTP-S11-based device (a), PM6:BTP-S12-based device (b), PM6:BTP-S9-based device (c), PM6:DAA-1-based device (d), PM6:DAA-2-based device (e), PM6:DAA-3-based device (f).

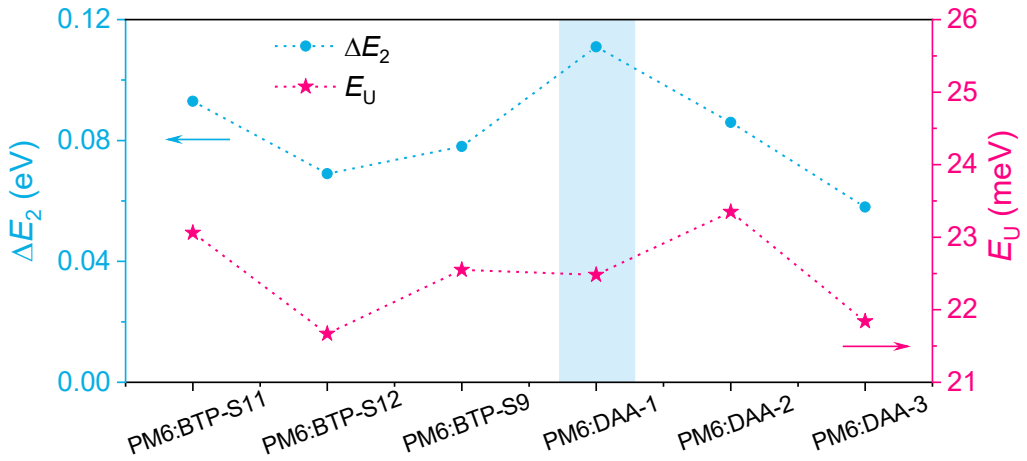

Fig. S32 Comparison of ΔE_2 and E_U for relevant binary and ternary OPVs.

Note S2: Boltzmann equilibrium

Fig. 5a shows the kinetic process involved with LE, CT and CS states, the non-radiative recombination loss will mainly happen on LE or CT states, particularly for CT states. Thus, the effective way for mitigating non-radiative loss is reducing the CT ratio. Accordingly, the Boltzmann equilibrium between LE and CT states will largely affect the CT ratio.

According to the Boltzmann probability distribution, the relative occupation of LE and CT states can be expressed as:

$$p_{LE} = \frac{g_1}{Q}\exp\left(-\frac{E_{LE}}{k_B T}\right);\ p_{CT} = \frac{g_2}{Q}\exp\left(-\frac{E_{CT}}{k_B T}\right) \qquad (6)$$

where Q is the canonical partition function, E_{LE} and E_{CT} are the energies of LE and CT states, k_B is the Boltzmann constant, and T is the temperature in Kelvin.

Then, the equilibrium constant K can be calculated as:

$$K = \frac{p_{CT}}{p_{LE}} = \frac{g_2}{g_1}\exp\left(\frac{\Delta E_{LE-CT}}{k_B T}\right) \qquad (7)$$

where $\Delta E_{LE\text{-}CT} = E_{LE} - E_{CT}$.

Under the stationary state for the reaction LE$\Leftrightarrow$ CT, we can identify that:

$$K = \frac{k_{12}}{k_{21}} = \frac{g_2}{g_1}\exp\left(\frac{\Delta E_{LE-CT}}{k_B T}\right) \qquad (8)$$

With equation (8), we can conclude that, reducing $\Delta E_{LE\text{-}CT}$ will reduce the equilibrium constant K between LE and CT states, thus reducing CT ratio for non-radiative loss mitigation.

However, above conclusion is based on the prerequisite that only Boltzmann equilibrium between LE and CT states is considered. In our work, we observe an obvious non-radiative loss reduction, due to luminescence efficiency enhancement of over 2 times, while the energetic offset ($\Delta E_{LE\text{-}CT}$) is less changed, which doesn't conform to above conclusion. This indicates more process should be considered for the Boltzmann equilibrium analysis. For non-fullerene

acceptors, especially Y-series molecules, it's detected that self-separation of exciton directly from LE to CT states exists, thus the process between LE and CS states should also be considered for Boltzmann equilibrium analysis.

Similarly, the relative occupation of CS state can be expressed as:

$$p_{CS} = \frac{g_3}{Q}\exp\left(-\frac{E_{CS}}{k_B T}\right) \qquad (9)$$

where E_{CS} is the energy of CS state.

Then the modified equilibrium constant *K*' can be changed to:

$$K' = \frac{p_{CT}}{p_{LE} + p_{CS}} = \frac{g_2 \exp\left(-\frac{E_{CT}}{k_B T}\right)}{g_1 \exp\left(-\frac{E_{LE}}{k_B T}\right) + g_3 \exp\left(-\frac{E_{CS}}{k_B T}\right)}$$
$$= \frac{1}{g_{12}\exp\left(-\frac{\Delta E_{LE-CT}}{k_B T}\right) + g_{32}\exp\left(-\frac{\Delta E_{CS-CT}}{k_B T}\right)} \qquad (10)$$

Where $g_{12} = g_1/g_2$, $g_{32} = g_3/g_2$.

So, under the stationary state for the reaction CT⇔ LE⇨ CS, we can identify that:

$$K' = \frac{k_{12}}{k_{21} + k_{13}} = \frac{1}{g_{12}\exp\left(-\frac{\Delta E_{LE-CT}}{k_B T}\right) + g_{32}\exp\left(-\frac{\Delta E_{CS-CT}}{k_B T}\right)} \qquad (11)$$

According to equation (11), we can learn that, the reduction of K' will be determined by both $\Delta E_{\text{LE-CT}}$ and $\Delta E_{\text{CS-CT}}$. Thus, for small driving force systems, both $\Delta E_{\text{LE-CT}}$ and $\Delta E_{\text{CS-CT}}$ are critical for non-radiative loss mitigation. Besides, a reduction of $\Delta E_{\text{CS-CT}}$ may also promote the conversion rate (k_{23}) from CT state to CS state, thus further reducing the CT ratio. So, Boltzmann equilibrium among LE, CT and CS states should be responsible for the non-radiative loss mitigation in small driving force systems.

Note S3: $\Delta E_{CS\text{-}CT}$

As shown above, the variation of $\Delta E_{CS\text{-}CT}$ may also put an effect on the non-radiative loss. Now we analyze the possible factor affecting the $\Delta E_{CS\text{-}CT}$. For donor (D) / acceptor (A) systems, there exists energy level bending at the D/A interfaces, as shown in **Fig. 5b**. The happening of energy level bending at the D/A interfaces is due to the electrostatic interaction of charges with quadrupole moments of surrounding molecules.

The energy level bending phenomenon will result in a parameter named as interfacial bending energy (B), which can be expressed as:

$$B = B_h^D + B_h^A = B_e^D + B_e^A \qquad (12)$$

Thus, the dissociation energy of CT state can be expressed as:

$$\Delta E_{CS-CT} = E_{CS} - E_{CT} = E_{Coulomb}^{CT} - B \qquad (13)$$

So, we can learn that, enlarging the interfacial bending energy could be a way to reduce $\Delta E_{CS\text{-}CT}$, thus being the factor for reducing CT state ratio and non-radiative recombination loss.

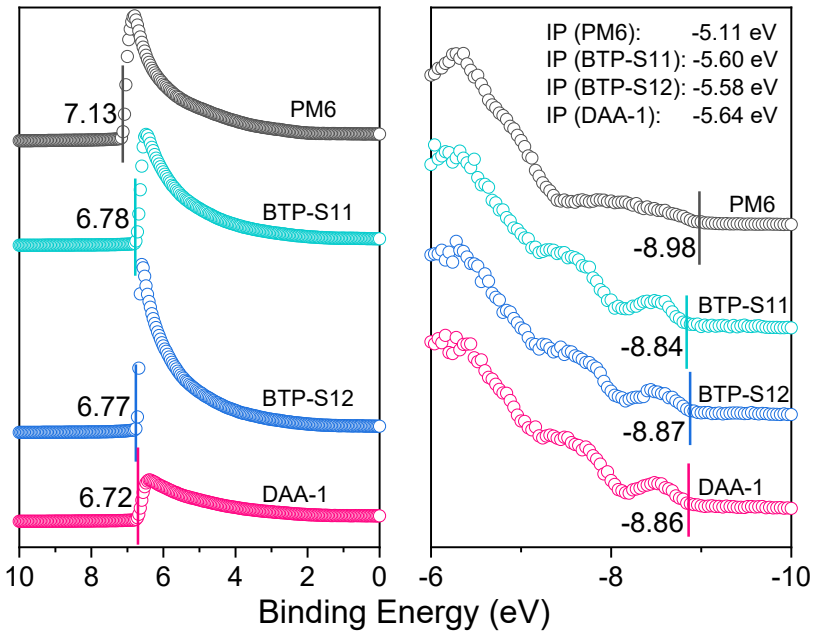

Fig. S33 Ultraviolet photoelectron spectroscopy (UPS) data of PM6, BTP-S11, BTP-S12 and DAA-1 neat films (He I; hν = 21.22 eV).

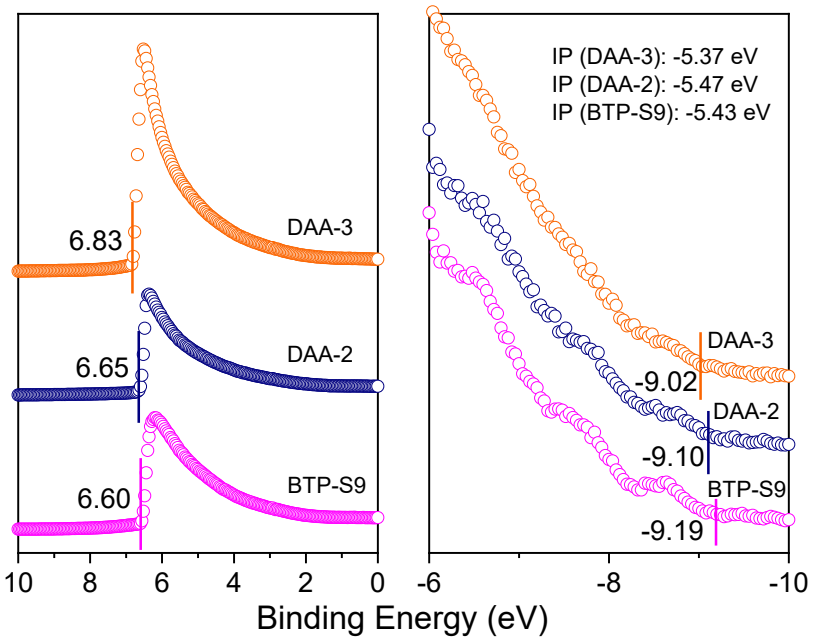

Fig. S34 Ultraviolet photoelectron spectroscopy (UPS) data of BTP-S9, DAA-2, and DAA-3 neat films (He I; hν = 21.22 eV).

Note S4: Interfacial bending energy (*B*)

As analyzed above, reducing $\Delta E_{\text{CS-CT}}$ will require an increase of interfacial bending energy (*B*). To accurately calculate the interfacial bending energy, we measured the ionization potential (IP) energy levels for PM6, BTP-S11, BTP-S12, BTP-S9, DAA-1, DAA-2 and DAA-3 neat films via ultraviolet photoelectron spectroscopy (UPS), and the results are displayed in **Figs. S33-34**. The IP values are calculated as -5.11 eV for PM6, -5.60 eV for BTP-S11, -5.58 eV for BTP-S12, -5.43 eV for BTP-S9, -5.64 eV for DAA-1, -5.47 eV for DAA-2 and -5.37 eV for DAA-3.

Since the energetic offset can be expressed as:

$$\Delta E_{LE-CT} = \Delta IP - B \qquad (14)$$

We can then calculate the bending energy *B* via the following equation:

$$B = \Delta IP - \Delta E_{LE-CT} \qquad (15)$$

Since the ΔIP values are found to be 0.49 eV for PM6:BTP-S11 system, 0.47 eV for PM6:BTP-S12 system, 0.32 eV for PM6:BTP-S9 system, 0.53 eV for PM6:DAA-1 system, 0.36 eV for PM6:DAA-2 system and 0.26 eV for PM6:DAA-3 system, then the bending energy *B* can be obtained as 0.439 eV for PM6:BTP-S11 system, 0.418 eV for PM6:BTP-S12 system, 0.279 eV for PM6:BTP-S9 system, 0.477 eV for PM6:DAA-1 system, 0.314 eV for PM6:DAA-2 system and 0.217 eV for PM6:DAA-3 system. The above results are also summarized in **Table S4**.

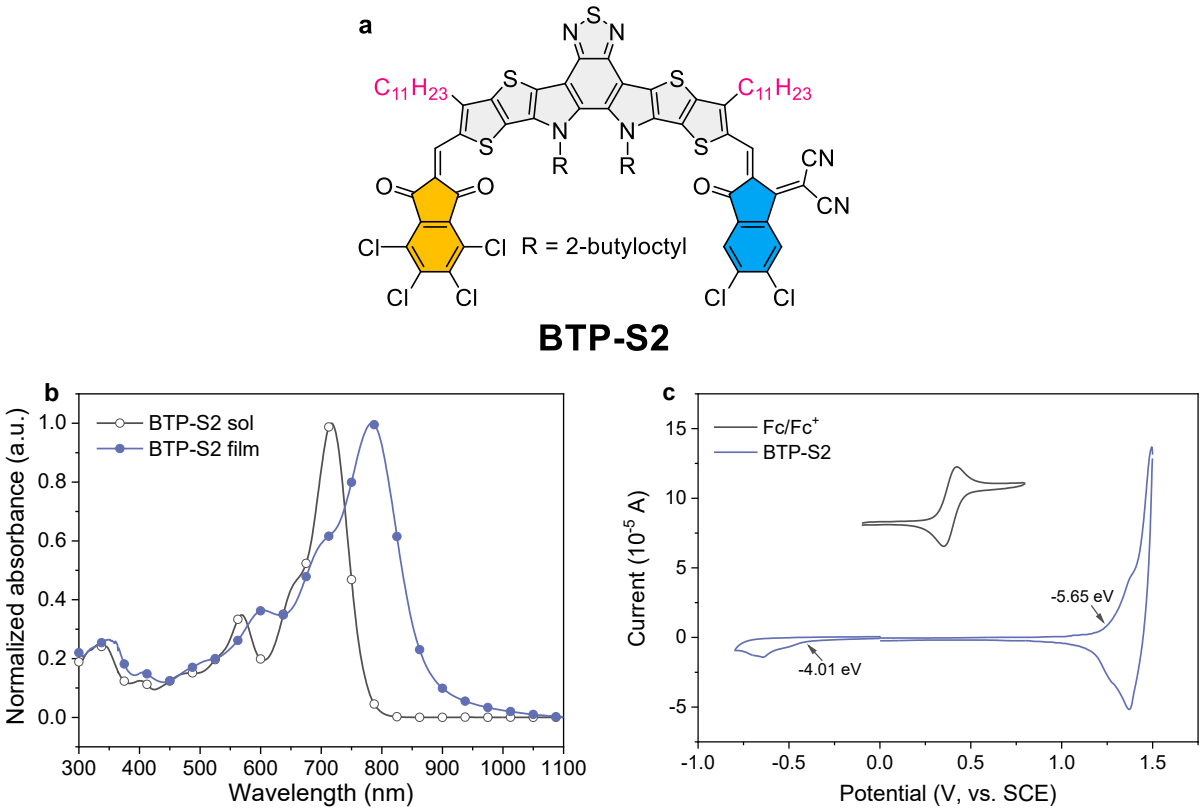

Fig. S35 (a) Chemical structure of BTP-S2. (b) Absorption spectra of BTP-S2 solution and film. (c) Cyclic voltammograms of BTP-S2.

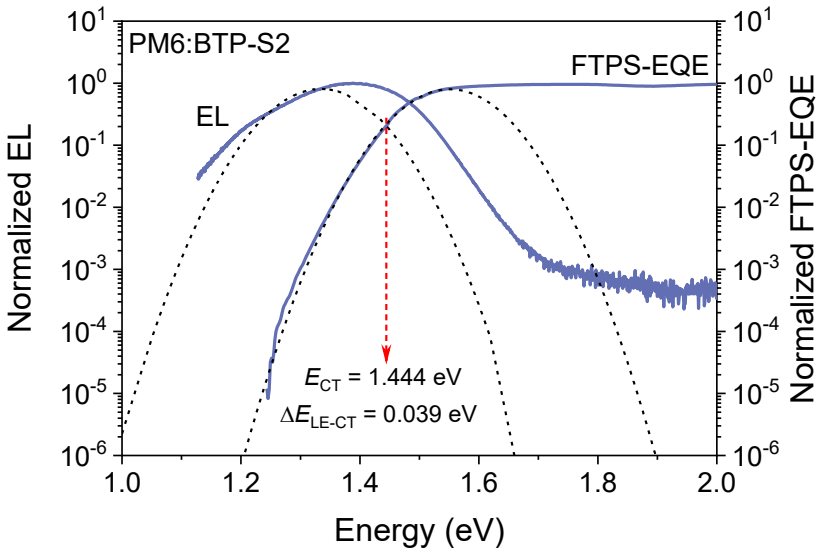

Fig. S36 Semilogarithmic plots of normalized EL and normalized FTPS-EQE (solid lines), and the determination of E_{CT} via Gaussian fits to EL and FTPS-EQE spectra according to the Marcus equation (dash lines) for PM6:BTP-S2-based device.

福建省计量科学研究院
FUJIAN METROLOGY INSTITUTE
（国家光伏产业计量测试中心）
National PV Industry Measurement and Testing Center

检 测 报 告
Test Report

报告编号：22Q3-00207
Report No.

客户名称 Name of Customer	Zhejiang University
联络信息 Contact Information	Hangzhou, Zhejiang Province, China
物品名称 Name of items	Organic Photovoltaics
型号/规格 Type /Specification	Non-fullerene OPV
物品编号 Items No	No. 16
制造厂商 Manufacturer	Zhejiang University
物品接收日期 Items Receipt Date	2022-10-21
检测日期 Test Date	2022-10-26

批准人 Approved by 黎健生
核验员 Checked by 何翔
检测员 Test by 陈彩云

发布日期 Date of Report 2022 年 Year 11 月 month 14 日 Day

扫一扫 查真伪

本院/本中心地址：福州市屏东路 9-3 号 Address：9-3 Pingdong Road,Fuzhou,China
电话：0591-87845050 Telephone
传真：0591-87808417 Fax
邮编：350003 Post Code
网址：www.fjjl.net Web Site
咨询电话：0591-87845050 Inquire line
投诉电话：0591-87823025 Complaint Tel

未经本院/本中心书面批准，部分复制采用本报告内容无效。
Partly using this Report will not be admitted unless allowed by FMI/ Center.

第 1 页/共 7 页 Page of Pages

Fig. S37 The copy of certified report from National PV Industry Measurement and Testing Center (NPVIM) for quaternary device (PM6:TAA-1 based quaternary OPV).

福建省计量科学研究院
FUJIAN METROLOGY INSTITUTE
（国家光伏产业计量测试中心）
National PV Industry Measurement and Testing Center

报告编号：22Q3-00207
Report No.

1. 检测机构说明：
Testing institutions that

本院为国家法定计量检定机构，国家光伏产业计量测试中心依托本院检测技术开展检测。本院/本中心质量管理体系符合 GB/T 27025（ISO/IEC 17025，IDT）标准要求。

The institute is a national legal metrological institution. National PV Industry Measurement and Testing Center carrys out testing relying on the institute's testing technology. The Center's quality management system meets the requirements of GB/T 27025（ISO/IEC 17025，IDT）standard.

2. 本次检测所依据的检测方法（代号及名称）：
Reference documents from the test (code.name)

IEC 60904-1-2020 光伏器件-第一部分：光伏电流-电压特性的测量;IEC 60904-8:2014 光伏器件-第 8 部分光伏器件的光谱响应度测量

3. 本次检测所使用的主要测量仪器：
Measurement standards used in this test

仪器名称 Name	仪器编号 Number	测量范围 Measuring Range	不确定度/或准确度等级/或最大允许误差 Uncertainty or Accuracy Class or Maximum Permissible Error	溯源机构名称/证书编号 Name of traceability Institution/Certificate No.	有效期限 Due date
源表	10807C008 78-2	电流：-10 μA~1A；电压：20mV~20V	测量：DCV:U_{rel}=0.05%，k=2； DCI:U_{rel}=0.05%，k=2 输出：DCV:U_{rel}=0.05%，k=2； DCI:U_{rel}=0.05%，k=2	福建计量院 22D2-01826	2023-04-13
太阳模拟器	2015-006	(300～1200) nm；(800～1200) W/m²	光谱匹配度(300～310) nm:U_{rel}=7.4% (k=2);(310～400) nm:U_{rel}=6.4% (k=2);(400～1200) nm:U_{rel}=5.5% (k=2);辐照度比 U_{rel}=1.2% (k=2)	福建计量院 22Q2-00720	2023-06-16
WPVS 单晶硅标准电池	015-2014	(300～1200) nm	U_{rel}=1.3% (k=2)	中国计量院 GXgf2021-10725	2023-04-05
Si 光电探测器	Si-2	(300～1100)nm	(300～400)nm U_{rel}=1.8%～1.7% (k=2)；(400～450)nm U_{rel}=1.7%～1.3% (k=2)；(450～1000)nm U_{rel}=1.3%～1.2% (k=2)；(1000～1100)nm U_{rel}=1.2%～1.7% (k=2)	中国计量院 GXgf2021-10903	2023-03-24
数字温度计	15-B	(15～65)℃	U=0.060 ℃ (k=2)	福建计量院 22B2-07588	2023-06-20

4. 检测地点及环境条件：
Location and environmental condition for the test

地点：Room 108, Building 4, MinHou Scientific Research Base
Location

温度：24.8 ℃ Temperature　　相对湿度：39 % Relative Humidity　　其它：/ Others

5. 备注：/
Note

本报告提供的结果仅对本次被检的物品有效。
The data are valid only for the instrument(s) under testing.

检测报告续页专用
Continued page of test report

第 2 页/共 7 页
Page of Pages

Fig. S37-continued The copy of certified report from National PV Industry Measurement and Testing Center (NPVIM) for quaternary device (PM6:TAA-1 based quaternary OPV).

福建省计量科学研究院
FUJIAN METROLOGY INSTITUTE
（国家光伏产业计量测试中心）
National PV Industry Measurement and Testing Center

报告编号：22Q3-00207
Report No.

检测结果/说明：
Results of Test and Additional Explanation.

1 Standard Test Condition (STC)： Total Irradiance： 1000 W/m^2
Temperature： 25.0 ℃
Spectral Distribution： AM1.5G

2 Measurement Data and I-V/P-V Curves under STC

Forward Scan

I_{sc} (mA)	V_{oc} (V)	I_{MPP} (mA)	V_{MPP} (V)	P_{MPP} (mW)	FF (%)	η (%)
1.255	0.8842	1.159	0.7591	0.8798	79.28	19.24

Reverse Scan

I_{sc} (mA)	V_{oc} (V)	I_{MPP} (mA)	V_{MPP} (V)	P_{MPP} (mW)	FF (%)	η (%)
1.257	0.8849	1.156	0.7626	0.8816	79.26	19.28

Mismatch Factor: 0.9927

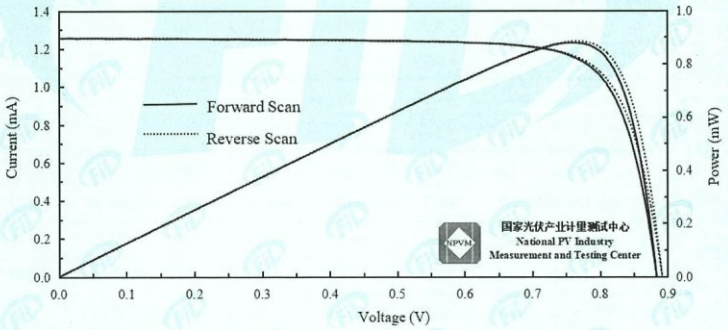

Figure 1. I-V and P-V characteristic curves of the measured sample under STC

检测报告续页专用
Continued page of test report

第 3 页/共 7 页
Page of Pages

Fig. S37-continued The copy of certified report from National PV Industry Measurement and Testing Center (NPVIM) for quaternary device (PM6:TAA-1 based quaternary OPV).

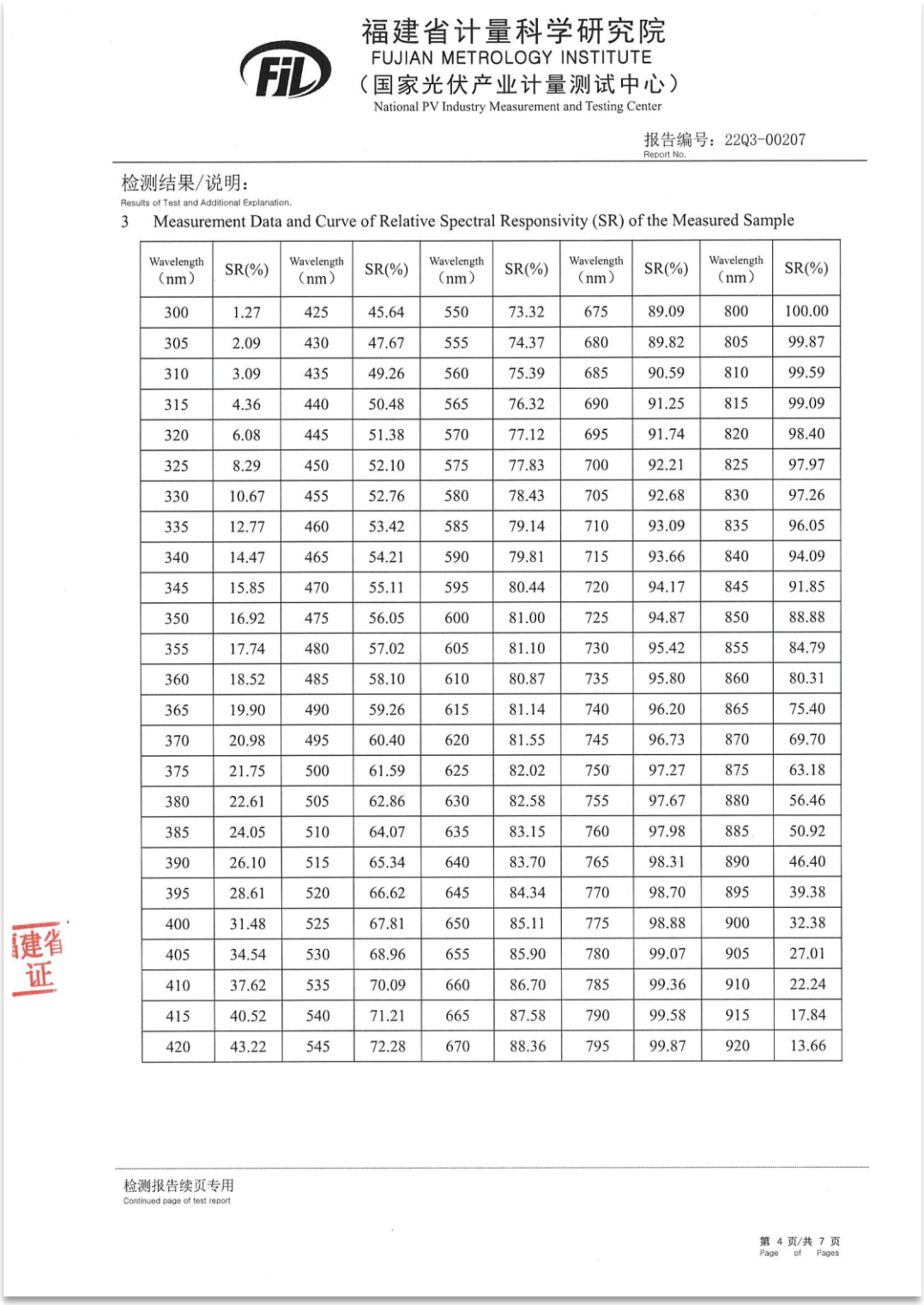

福建省计量科学研究院
FUJIAN METROLOGY INSTITUTE
（国家光伏产业计量测试中心）
National PV Industry Measurement and Testing Center

报告编号：22Q3-00207
Report No.

检测结果/说明：
Results of Test and Additional Explanation.

3 Measurement Data and Curve of Relative Spectral Responsivity (SR) of the Measured Sample

Wavelength (nm)	SR(%)	Wavelength (nm)	SR(%)	Wavelength (nm)	SR(%)	Wavelength (nm)	SR(%)	Wavelength (nm)	SR(%)
300	1.27	425	45.64	550	73.32	675	89.09	800	100.00
305	2.09	430	47.67	555	74.37	680	89.82	805	99.87
310	3.09	435	49.26	560	75.39	685	90.59	810	99.59
315	4.36	440	50.48	565	76.32	690	91.25	815	99.09
320	6.08	445	51.38	570	77.12	695	91.74	820	98.40
325	8.29	450	52.10	575	77.83	700	92.21	825	97.97
330	10.67	455	52.76	580	78.43	705	92.68	830	97.26
335	12.77	460	53.42	585	79.14	710	93.09	835	96.05
340	14.47	465	54.21	590	79.81	715	93.66	840	94.09
345	15.85	470	55.11	595	80.44	720	94.17	845	91.85
350	16.92	475	56.05	600	81.00	725	94.87	850	88.88
355	17.74	480	57.02	605	81.10	730	95.42	855	84.79
360	18.52	485	58.10	610	80.87	735	95.80	860	80.31
365	19.90	490	59.26	615	81.14	740	96.20	865	75.40
370	20.98	495	60.40	620	81.55	745	96.73	870	69.70
375	21.75	500	61.59	625	82.02	750	97.27	875	63.18
380	22.61	505	62.86	630	82.58	755	97.67	880	56.46
385	24.05	510	64.07	635	83.15	760	97.98	885	50.92
390	26.10	515	65.34	640	83.70	765	98.31	890	46.40
395	28.61	520	66.62	645	84.34	770	98.70	895	39.38
400	31.48	525	67.81	650	85.11	775	98.88	900	32.38
405	34.54	530	68.96	655	85.90	780	99.07	905	27.01
410	37.62	535	70.09	660	86.70	785	99.36	910	22.24
415	40.52	540	71.21	665	87.58	790	99.58	915	17.84
420	43.22	545	72.28	670	88.36	795	99.87	920	13.66

检测报告续页专用
Continued page of test report

第 4 页/共 7 页
Page of Pages

Fig. S37-continued The copy of certified report from National PV Industry Measurement and Testing Center (NPVIM) for quaternary device (PM6:TAA-1 based quaternary OPV).

福建省计量科学研究院
FUJIAN METROLOGY INSTITUTE
（国家光伏产业计量测试中心）
National PV Industry Measurement and Testing Center

报告编号：22Q3-00207
Report No.

检测结果/说明：
Results of Test and Additional Explanation.

Wavelength（nm）	SR(%)	Wavelength（nm）	SR(%)	Wavelength（nm）	SR(%)	Wavelength（nm）	SR(%)	Wavelength（nm）	SR(%)
925	11.28	945	3.91	965	1.46	985	0.44	/	/
930	9.09	950	3.10	970	1.13	990	0.37	/	/
935	6.95	955	2.41	975	0.83	995	0.29	/	/
940	5.11	960	1.85	980	0.58	1000	0.22	/	/

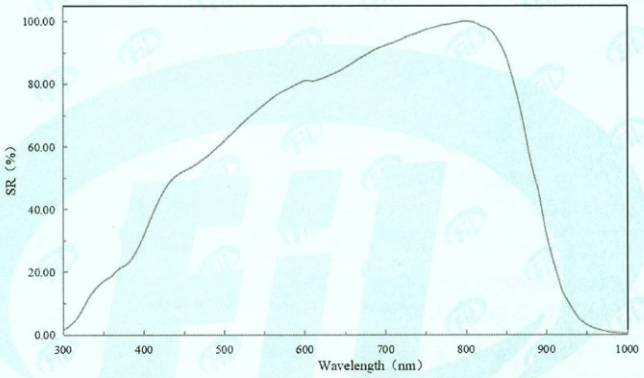

Figure 2. Relative spectral responsivity curve of the measured sample

4 Pictures of the Measured Sample

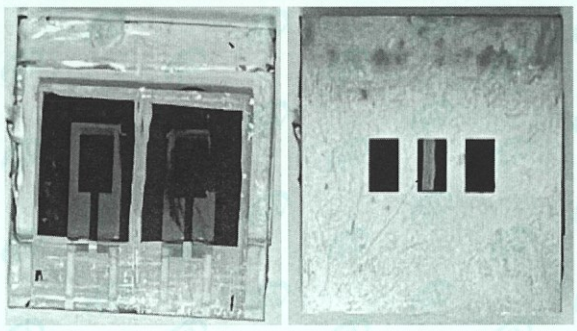

Figure 3. Mask used during test and obverse side of the sample

检测报告续页专用
Continued page of test report

第 5 页/共 7 页
Page of Pages

Fig. S37-continued The copy of certified report from National PV Industry Measurement and Testing Center (NPVIM) for quaternary device (PM6:TAA-1 based quaternary OPV).

福建省计量科学研究院
FUJIAN METROLOGY INSTITUTE
（国家光伏产业计量测试中心）
National PV Industry Measurement and Testing Center

报告编号：22Q3-00207
Report No.

检测结果/说明：
Results of Test and Additional Explanation.

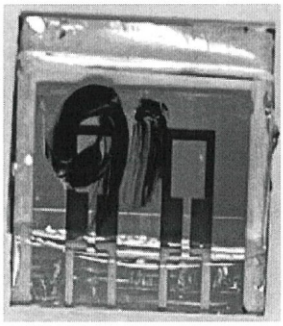

Figure 4. Reverse side of the measured sample

Uncertainty of Measurement Results:

Short-Circuit Current: U_{rel}=1.8% (k=2); Open-Circuit Voltage: U_{rel}=1.0% (k=2);

Maximum Power: U_{rel}=2.2% (k=2); Efficiency: U_{rel}=2.2% (k=2); Fill Factor: U_{rel}=3.2% (k=2).

Relative Spectral Responsivity:

(300~400) nm: U_{rel} = 2.2% (k=2);

(400~1000) nm: U_{rel} = 1.8% (k=2);

说明：The designated illuminated area of the measured sample was 0.04572 cm^2.
Explanation

Testing Method (Code and Name) for This Test
IEC 60904-1: 2020 Photovoltaic devices- Part 1: Measurement of photovoltaic current-voltage characteristics
IEC 60904-8: 2014 Photovoltaic devices- Part 8: Measurement of spectral responsivity of a photovoltaic (PV) device

计量科
书 骑

检测报告续页专用
Continued page of test report

第 6 页/共 7 页
Page of Pages

Fig. S37-continued The copy of certified report from National PV Industry Measurement and Testing Center (NPVIM) for quaternary device (PM6:TAA-1 based quaternary OPV).

福建省计量科学研究院
FUJIAN METROLOGY INSTITUTE
（国家光伏产业计量测试中心）
National PV Industry Measurement and Testing Center

报告编号：22Q3-00207
Report No.

检测结果/说明：
Results of Test and Additional Explanation.

Measurement Standards Used in This Test					
Name	**Number**	**Measuring Range**	**Uncertainty or Accuracy Class or Maximum Permissible Error**	**Name of Traceability Institution/Certificate No.**	**Due Date**
SourceMeter	10807C0087 8-2	DCI: (-10μA~1A); DCV: (20mV~20V)	Measure: DCV:U_{rel}=0.05%,k=2; DCI: U_{rel}=0.05%,k=2 Output: DCV:U_{rel}=0.05%,k=2; DCI: U_{rel}=0.05%,k=2	Fujian Metrology Institute/ 22D2-01826	2023-04-13
Solar Simulator	2015-006	(300～1200) nm; (800～1200) W/m^2	Spectral Match: (300～310) nm: U_{rel}=7.4% (k=2);(310～400) nm: U_{rel}=6.4% (k=2);(400～1200) nm: U_{rel}=5.5% (k=2);Irradiance Ratio: U_{rel}=1.2% (k=2)	Fujian Metrology Institute/ 22Q2-00720	2023-06-16
WPVS Monocrystalline Silicon Reference Cell	015-2014	(300～1200) nm	U_{rel}=1.3% (k=2)	National Institute of Metrology/ GXgf2021-10725	2023-04-05
Si Photoelectric Detector	Si-2	(300~1100) nm	(300～400) nm U_{rel}=1.8%～1.7% (k=2) ; (400～450) nm U_{rel}=1.7%～1.3% (k=2) ; (450～1000) nm U_{rel}=1.3%～1.2% (k=2) ; (1000～1100) nm U_{rel}=1.2%～1.7% (k=2)	National Institute of Metrology/ GXgf2021-10903	2023-03-24
Digital Thermometer	15-B	(15～65) ℃	U=0.060 ℃ (k=2)	Fujian Metrology Institute/22B2-07588	2023-06-20

以下空白
Blank below

检测报告续页专用
Continued page of test report

第 7 页/共 7 页
Page of Pages

Fig. S37-continued The copy of certified report from National PV Industry Measurement and Testing Center (NPVIM) for quaternary device (PM6:TAA-1 based quaternary OPV).

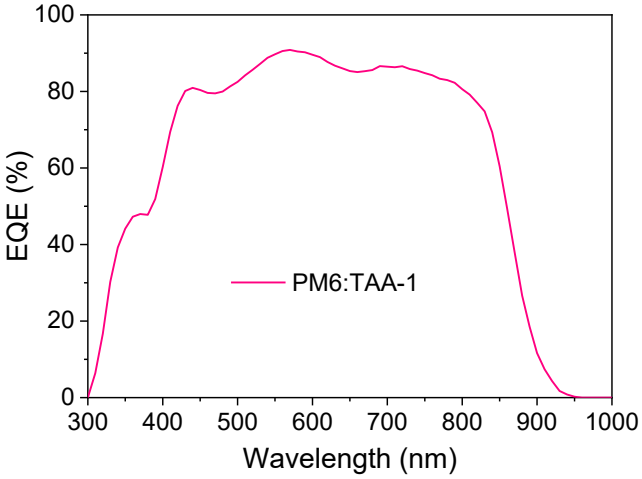

Fig. S38 EQE curve of device based on PM6:TAA-1 blend (TAA-1: BTP-S11:BTP-S12:BTP-S2 = 0.7:0.3:0.2).

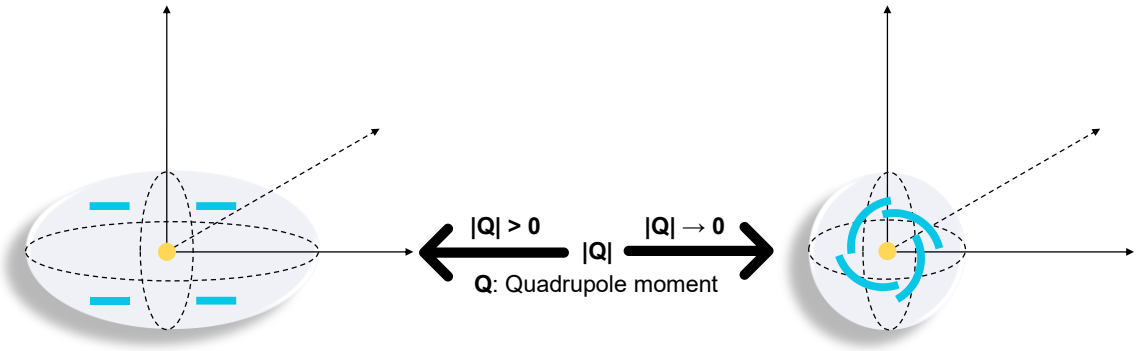

Fig. S39 Diagram of varied quadrupole moments with increased straight-crystal or curved-crystal.

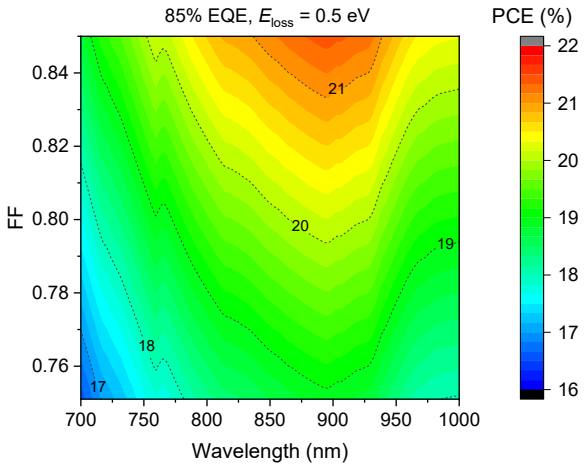

Fig. S40 Efficiency potentials of OPVs with the change of FF.

Supplementary Tables

Table S1 Summary of photovoltaic parameters of binary and ternary OPVs for this work and reported references

Device type	Active layer	V_{oc} (V)	J_{sc} (mA cm^{-2})	FF (%)	V_{oc} * J_{sc}	PCE (%)	Ref.
Binary	PM6:BTP-S11	0.878	27.1	79.3	23.79	18.9	This work
	PM6:Y6	0.830	25.3	74.8	21.00	15.7	[1]
	PM6:BTP-4Cl	0.867	25.4	75.0	22.02	16.5	[2]
	PM6:BO-4Cl	0.858	25.6	77.6	21.96	17.0	[3]
	PM6:BTP-4F-12	0.855	25.3	76.0	21.63	16.4	[4]
	PM6:N3	0.837	25.8	73.9	21.59	16.0	[5]
	PM6:BTP-eC9	0.839	26.2	81.1	21.98	17.8	[6]
	PM6:BTP-S2	0.945	24.1	72.0	22.77	16.4	[7]
	PM6:AQx-2	0.860	25.4	76.3	21.84	16.6	[8]
	PM6:BTIC-2Br-m	0.880	25.0	73.1	22.00	16.1	[9]
	PM6:DTY6	0.858	25.3	75.4	21.71	16.3	[10]
	PM6:BTIC-CF_3-g	0.850	25.2	72.8	21.42	15.6	[11]
	PM6:BTP-2F-ThCl	0.869	25.4	77.4	22.07	17.1	[12]
	PM6:Y6-O	0.940	22.9	77.0	21.53	16.5	[13]
	PM6:Y11	0.833	26.7	74.3	22.24	16.5	[14]
	PM6:mBzS-4F	0.804	27.7	76.4	22.27	17.0	[15]
	PM6:BTP-4F-P2EH	0.880	25.9	80.1	22.79	18.2	[16]
	PM6:A-WSSe-Cl	0.850	26.6	77.5	22.61	17.5	[17]
	PM6:BT-BO-L4F	0.830	28.4	70.3	23.57	16.6	[18]
	PM6:BTP-S9	0.846	26.5	78.4	22.42	17.6	[19]
	PM6:L8-BO	0.870	25.7	81.5	22.36	18.3	[20]
	PM6:EH-HD-4F	0.840	27.5	79.3	23.10	18.4	[21]
	PTQ10:Y6	0.870	24.8	75.1	21.58	16.2	[22]
	Pt10:Y6	0.810	26.5	76.3	21.47	16.4	[23]
	P2F-EHp:Y6	0.810	26.7	74.1	21.63	16.0	[24]
	PM6-Ir1:Y6	0.845	26.2	78.4	22.14	17.3	[25]
	PBTT-F:Y6	0.840	24.8	77.1	20.83	16.1	[26]
	PTQ11:TPT10	0.880	24.8	74.8	21.82	16.3	[27]
	D18:Y6Se	0.839	28.0	75.3	23.49	17.7	[28]
	PT2:Y6	0.830	26.7	74.4	22.16	16.5	[29]
	PM1:Y6	0.870	25.9	78.0	22.53	17.6	[30]
	D18:Y6	0.859	27.7	76.6	23.79	18.2	[31]
	PM7:Y6	0.897	25.6	74.0	22.96	17.0	[32]
	PBTATBT-4f:Y6	0.810	27.3	72.7	22.11	16.1	[33]
	SZ4:N3	0.848	26.0	77.4	22.05	16.7	[34]

	PBQ10:Y6	0.850	25.8	74.6	21.93	16.3	[35]
	P5T:BTP-eC9	0.837	26.5	79.8	22.18	17.7	[36]
	PBQ6:Y6	0.851	26.6	77.9	22.64	17.6	[37]
	PM6-Tz20:Y6	0.860	27.3	75.0	23.48	17.6	[38]
	PBNT-BDD:Y6	0.880	25.4	72.0	22.35	16.1	[39]
	PTVT-T:BTP-eC9	0.790	26.2	78.0	20.70	16.2	[40]
	PBDB-T:PN-Se	0.907	24.8	71.8	22.49	16.2	[41]
	D18:BO-4Cl	0.860	26.3	77.7	22.62	17.6	[42]
	PTQ10:m-BTP-C6Ph	0.883	25.3	79.3	22.34	17.7	[43]
	PNTB6-Cl:N3	0.857	26.6	77.3	22.80	17.6	[44]
	PBCT-2F:Y6	0.850	27.2	74.3	23.12	17.1	[45]
Ternary	PM6:DAA-4	0.880	27.1	79.9	23.85	19.1	This work
	PM6:Y6:$PC_{71}BM$	0.850	25.8	74.7	21.93	16.4	[46]
	PM6:Y6:BTTPC	0.860	25.5	77.0	21.93	16.8	[47]
	PM6:Y6:BTP-M	0.875	26.6	73.5	23.28	17.0	[48]
	PM6:Y18:$PC_{71}BM$	0.840	26.3	77.4	22.09	17.1	[49]
	PM6:CH1007:$PC_{71}BM$	0.822	27.5	75.6	22.61	17.1	[50]
	PM6:BTP-4F-12:MeIC	0.863	25.4	79.2	21.92	17.4	[51]
	PM6:PB2F:BTP-eC9	0.863	26.8	80.4	23.13	18.6	[52]
	D18-Cl:Y6:$PC_{71}BM$	0.870	26.8	77.0	23.32	18.0	[53]
	D18-Cl:Y6:Y6-1O	0.900	25.9	76.9	23.31	17.9	[54]
	PM6:CH1007:BT-4BO	0.880	26.9	75.4	23.67	17.8	[55]
	PTQ10:BTP-Ph:BTP-Th	0.888	25.2	78.6	22.38	17.6	[56]
	PM6:Y6-1O:$PC_{71}BM$	0.900	24.9	78.5	22.41	17.6	[57]
	PTQ10:m-BTP-PhC6:$PC_{71}BM$	0.869	27.0	80.6	23.46	18.9	[58]
	PM6:BTP-eC9:L8-BO-F	0.853	27.4	80.0	23.37	18.7	[59]
	PBQx-TF:eC9-2Cl:F-BTA3	0.879	26.7	80.9	23.47	19.0	[60]
	PBQx-TCl:BTP-eC9:BTA3	0.840	26.9	79.6	22.60	18.0	[61]
	PM6:BO-4Cl:BTP-S2	0.861	27.1	78.0	23.33	18.2	[62]
	D18:Y6:BTPR	0.863	27.8	74.6	23.99	17.8	[63]
	PM6:BTP-eC9:BTP-F	0.858	27.0	79.7	23.17	18.5	[64]
	B1:BO-4Cl:BO-2Cl	0.840	26.1	78.0	21.92	17.0	[65]
	PM6:eC9:HDO-4Cl	0.866	27.1	80.5	23.47	18.9	[66]
	D18-Cl:Y6:G19	0.871	27.4	77.7	23.87	18.5	[67]
	PM6:PYT:PY2F-T	0.900	25.2	76.0	22.68	17.2	[68]
	PNTB-2T:Y6:$PC_{71}BM$	0.875	26.5	75.0	23.19	17.4	[69]

Table S2 Summary of hole and electron mobilities for binary and ternary devices

Active layer	μ_h ($\times10^{-3}$ cm^2 V^{-1} s^{-1})	μ_e ($\times10^{-3}$ cm^2 V^{-1} s^{-1})	μ_h / μ_e
PM6:BTP-S11	2.45±0.42	2.62±1.12	0.94
PM6:BTP-S12	1.09±0.18	0.33±0.15	3.30
PM6:BTP-S9	2.91±0.41	3.53±2.06	0.82
PM6:DAA-1	2.30±0.33	2.96±1.65	0.78
PM6:DAA-2	1.61±0.43	2.46±1.23	0.65
PM6:DAA-3	1.66±0.28	2.46±0.39	0.67
PM6:DAA-4	2.40±0.38	3.19±0.33	0.75

Table S3 Summary of miscibility and aggregation parameters

Material	θ_{water} (°)	$\theta_{diiodomethane}$ (°)	γ^d (mN m^{-1}) [a]	γ^h (mN m^{-1}) [b]	γ (mN m^{-1}) [c]	$\chi^{D\text{-}A}$ [d]	R_q (nm)
PM6	105.41	58.60	1.33	48.97	50.30	/	0.99
BTP-S11	94.31	46.82	3.08	55.33	58.41	0.30	0.55
BTP-S12	91.78	45.78	3.70	54.67	58.37	0.30	1.78
BTP-S9	94.28	42.91	2.87	59.65	62.52	0.66	0.57
DAA-1	94.86	44.62	2.81	58.20	61.01	0.52	0.67
DAA-2	95.55	46.85	2.76	56.20	58.96	0.34	0.69
DAA-3	95.47	46.48	2.76	56.56	59.32	0.37	0.52

[a] Surface tension from dipole-dipole component.

[b] Surface tension from hydrogen bond component.

[c] The total surface tension is calculated through the equation of $\gamma = \gamma^d + \gamma^h$.

[d] The Flory-Huggins interaction parameter between the donor (D) and acceptor (A) is calculated with the equation of $\chi^{D-A} = (\sqrt{\gamma_D} - \sqrt{\gamma_A})^2$.

Table S4 Summary of ΔIP, $\Delta E_{LE\text{-}CT}$, B, ΔE_3 and EQE_{EL} parameters for binary and ternary systems

Active Layer	ΔIP (eV)	$\Delta E_{LE\text{-}CT}$ (eV)	B (eV)	ΔE_3 (eV)	EQE_{EL} (10^{-2}%)
PM6:BTP-S11	0.49	0.051	0.439	0.194	4.12
PM6:BTP-S12	0.47	0.052	0.418	0.210	3.12
PM6:BTP-S9	0.32	0.041	0.279	0.201	3.17
PM6:DAA-1	0.53	0.053	0.477	0.179	8.67
PM6:DAA-2	0.36	0.046	0.314	0.190	6.38
PM6:DAA-3	0.26	0.043	0.217	0.199	3.62

Supplementary References

1 J. Yuan, Y. Zhang, L. Zhou, G. Zhang, H.-L. Yip, T.-K. Lau, X. Lu, C. Zhu, H. Peng, P. A. Johnson, M. Leclerc, Y. Cao, J. Ulanski, Y. Li and Y. Zou, *Joule*, 2019, **3**, 1140-1151.

2 Y. Cui, H. Yao, J. Zhang, T. Zhang, Y. Wang, L. Hong, K. Xian, B. Xu, S. Zhang, J. Peng, Z. Wei, F. Gao and J. Hou, *Nat. Commun.*, 2019, **10**, 2515.

3 Y. Cui, H. Yao, L. Hong, T. Zhang, Y. Tang, B. Lin, K. Xian, B. Gao, C. An, P. Bi, W. Ma and J. Hou, *Natl. Sci. Rev.*, 2019, **7**, 1239-1246.

4 L. Hong, H. Yao, Z. Wu, Y. Cui, T. Zhang, Y. Xu, R. Yu, Q. Liao, B. Gao, K. Xian, H. Y. Woo, Z. Ge and J. Hou, *Adv. Mater.*, 2019, **31**, 1903441.

5 K. Jiang, Q. Wei, J. Y. L. Lai, Z. Peng, H. K. Kim, J. Yuan, L. Ye, H. Ade, Y. Zou and H. Yan, *Joule*, 2019, **3**, 3020-3033.

6 Y. Cui, H. Yao, J. Zhang, K. Xian, T. Zhang, L. Hong, Y. Wang, Y. Xu, K. Ma, C. An, C. He, Z. Wei, F. Gao and J. Hou, *Adv. Mater.*, 2020, **32**, 1908205.

7 S. Li, L. Zhan, Y. Jin, G. Zhou, T.-K. Lau, R. Qin, M. Shi, C.-Z. Li, H. Zhu, X. Lu, F. Zhang and H. Chen, *Adv. Mater.*, 2020, **32**, 2001160.

8 Z. Zhou, W. Liu, G. Zhou, M. Zhang, D. Qian, J. Zhang, S. Chen, S. Xu, C. Yang, F. Gao, H. Zhu, F. Liu and X. Zhu, *Adv. Mater.*, 2020, **32**, 1906324.

9 H. Wang, T. Liu, J. Zhou, D. Mo, L. Han, H. Lai, H. Chen, N. Zheng, Y. Zhu, Z. Xie and F. He, *Adv. Sci.*, 2020, **7**, 1903784.

10 S. Dong, T. Jia, K. Zhang, J. Jing and F. Huang, *Joule*, 2020, **4**, 2004-2016.

11 H. Lai, Q. Zhao, Z. Chen, H. Chen, P. Chao, Y. Zhu, Y. Lang, N. Zhen, D. Mo, Y. Zhang and F. He, *Joule*, 2020, **4**, 688-700.

12 Z. Luo, R. Ma, T. Liu, J. Yu, Y. Xiao, R. Sun, G. Xie, J. Yuan, Y. Chen, K. Chen, G. Chai, H. Sun, J. Min, J. Zhang, Y. Zou, C. Yang, X. Lu, F. Gao and H. Yan, *Joule*, 2020, **4**, 1236-1247.

13 L.-K. Ma, Y. Chen, P. C. Y. Chow, G. Zhang, J. Huang, C. Ma, J. Zhang, H. Yin, A. M. Hong Cheung, K. S. Wong, S. K. So and H. Yan, *Joule*, 2020, **4**, 1486-1500.

14 S. Liu, J. Yuan, W. Deng, M. Luo, Y. Xie, Q. Liang, Y. Zou, Z. He, H. Wu and Y. Cao, *Nat. Photonics*, 2020, **14**, 300-305.

15 F. Qi, K. Jiang, F. Lin, Z. Wu, H. Zhang, W. Gao, Y. Li, Z. Cai, H. Y. Woo, Z. Zhu and A. K. Y. Jen, *ACS Energy Lett.*, 2021, **6**, 9-15.

16 J. Zhang, F. Bai, I. Angunawela, X. Xu, S. Luo, C. Li, G. Chai, H. Yu, Y. Chen, H. Hu, Z. Ma, H. Ade and H. Yan, *Adv. Energy Mater.*, 2021, **11**, 2102596.

17 C. Yang, Q. An, H.-R. Bai, H.-F. Zhi, H. S. Ryu, A. Mahmood, X. Zhao, S. Zhang, H. Y. Woo and J.-L. Wang, *Angew. Chem. Int. Ed.*, 2021, **60**, 19241-19252.

18 G. Li, X. Zhang, L. O. Jones, J. M. Alzola, S. Mukherjee, L.-w. Feng, W. Zhu, C. L. Stern, W. Huang, J. Yu, V. K. Sangwan, D. M. DeLongchamp, K. L. Kohlstedt, M. R. Wasielewski, M. C. Hersam, G. C. Schatz, A. Facchetti and T. J. Marks, *J. Am. Chem. Soc.*, 2021, **143**, 6123-6139.

19 S. Li, L. Zhan, N. Yao, X. Xia, Z. Chen, W. Yang, C. He, L. Zuo, M. Shi, H. Zhu, X. Lu, F. Zhang and H. Chen, *Nat. Commun.*, 2021, **12**, 4627.

20 C. Li, J. Zhou, J. Song, J. Xu, H. Zhang, X. Zhang, J. Guo, L. Zhu, D. Wei, G. Han, J. Min, Y. Zhang, Z. Xie, Y. Yi, H. Yan, F. Gao, F. Liu and Y. Sun, *Nat. Energy*, 2021, **6**, 605-613.

21 S. Chen, L. Feng, T. Jia, J. Jing, Z. Hu, K. Zhang and F. Huang, *Sci. China Chem.*, 2021, **64**, 1192-1199.
22 C. Sun, F. Pan, S. Chen, R. Wang, R. Sun, Z. Shang, B. Qiu, J. Min, M. Lv, L. Meng, C. Zhang, M. Xiao, C. Yang and Y. Li, *Adv. Mater.*, 2019, **31**, 1905480.
23 X. Xu, K. Feng, Z. Bi, W. Ma, G. Zhang and Q. Peng, *Adv. Mater.*, 2019, **31**, 1901872.
24 B. Fan, D. Zhang, M. Li, W. Zhong, Z. Zeng, L. Ying, F. Huang and Y. Cao, *Sci. China Chem.*, 2019, **62**, 746-752.
25 T. Wang, R. Sun, M. Shi, F. Pan, Z. Hu, F. Huang, Y. Li and J. Min, *Adv. Energy Mater.*, 2020, **10**, 2000590.
26 P. Chao, H. Chen, Y. Zhu, H. Lai, D. Mo, N. Zheng, X. Chang, H. Meng and F. He, *Adv. Mater.*, 2020, **32**, 1907059.
27 C. Sun, S. Qin, R. Wang, S. Chen, F. Pan, B. Qiu, Z. Shang, L. Meng, C. Zhang, M. Xiao, C. Yang and Y. Li, *J. Am. Chem. Soc.*, 2020, **142**, 1465-1474.
28 Z. Zhang, Y. Li, G. Cai, Y. Zhang, X. Lu and Y. Lin, *J. Am. Chem. Soc.*, 2020, **142**, 18741-18745.
29 K. Weng, L. Ye, L. Zhu, J. Xu, J. Zhou, X. Feng, G. Lu, S. Tan, F. Liu and Y. Sun, *Nat. Commun.*, 2020, **11**, 2855.
30 J. Wu, G. Li, J. Fang, X. Guo, L. Zhu, B. Guo, Y. Wang, G. Zhang, L. Arunagiri, F. Liu, H. Yan, M. Zhang and Y. Li, *Nat. Commun.*, 2020, **11**, 4612.
31 Q. Liu, Y. Jiang, K. Jin, J. Qin, J. Xu, W. Li, J. Xiong, J. Liu, Z. Xiao, K. Sun, S. Yang, X. Zhang and L. Ding, *Sci. Bull.*, 2020, **65**, 272-275.
32 M. Ruijie, L. Tao, L. Zhenghui, G. Qing, X. Yiqun, C. Yuzhong, L. Xiaojun, L. Siwei, L. Xinhui, Z. Maojie, L. Yongfang and Y. He, *Sci. China Chem.*, 2020, **63**, 325-330.
33 L.-W. Feng, J. Chen, S. Mukherjee, V. K. Sangwan, W. Huang, Y. Chen, D. Zheng, J. W. Strzalka, G. Wang, M. C. Hersam, D. DeLongchamp, A. Facchetti and T. J. Marks, *ACS Energy Lett.*, 2020, **5**, 1780-1787.
34 J. Liang, M. Pan, G. Chai, Z. Peng, J. Zhang, S. Luo, Q. Han, Y. Chen, A. Shang, F. Bai, Y. Xu, H. Yu, J. Y. L. Lai, Q. Chen, M. Zhang, H. Ade and H. Yan, *Adv. Mater.*, 2020, **32**, 2003500.
35 C. Sun, F. Pan, B. Qiu, S. Qin, S. Chen, Z. Shang, L. Meng, C. Yang and Y. Li, *Chem. Mater.*, 2020, **32**, 3254-3261.
36 L. Ma, S. Zhang, J. Wang, J. Ren, M. Gao, J. Zhang, T. Zhang, H. Yao, L. Ye and J. Hou, *ACS Mater. Lett.*, 2021, **3**, 1276-1283.
37 C. Zhu, L. Meng, J. Zhang, S. Qin, W. Lai, B. Qiu, J. Yuan, Y. Wan, W. Huang and Y. Li, *Adv. Mater.*, 2021, **33**, 2100474.
38 X. Guo, Q. Fan, J. Wu, G. Li, Z. Peng, W. Su, J. Lin, L. Hou, Y. Qin, H. Ade, L. Ye, M. Zhang and Y. Li, *Angew. Chem. Int. Ed.*, 2021, **60**, 2322-2329.
39 S. Pang, Z. Wang, X. Yuan, L. Pan, W. Deng, H. Tang, H. Wu, S. Chen, C. Duan, F. Huang and Y. Cao, *Angew. Chem. Int. Ed.*, 2021, **60**, 8813-8817.
40 J. Ren, P. Bi, J. Zhang, J. Liu, J. Wang, Y. Xu, Z. Wei, S. Zhang and J. Hou, *Natl. Sci. Rev.*, 2021, **8**, nwab031.
41 J. Du, K. Hu, J. Zhang, L. Meng, J. Yue, I. Angunawela, H. Yan, S. Qin, X. Kong, Z. Zhang, B. Guan, H. Ade and Y. Li, *Nat. Commun.*, 2021, **12**, 5264.
42 H. Chen, T. Zhao, L. Li, P. Tan, H. Lai, Y. Zhu, X. Lai, L. Han, N. Zheng, L. Guo and F.

He, *Adv. Mater.*, 2021, **33**, 2102778.
43 G. Chai, Y. Chang, J. Zhang, X. Xu, L. Yu, X. Zou, X. Li, Y. Chen, S. Luo, B. Liu, F. Bai, Z. Luo, H. Yu, J. Liang, T. Liu, K. S. Wong, H. Zhou, Q. Peng and H. Yan, *Energy Environ. Sci.*, 2021, **14**, 3469-3479.
44 H. Ning, Q. Jiang, P. Han, M. Lin, G. Zhang, J. Chen, H. Chen, S. Zeng, J. Gao, J. Liu, F. He and Q. Wu, *Energy Environ. Sci.*, 2021, **14**, 5919-5928.
45 X. Yuan, Y. Zhao, T. Zhan, J. Oh, J. Zhou, J. Li, X. Wang, Z. Wang, S. Pang, P. Cai, C. Yang, Z. He, Z. Xie, C. Duan, F. Huang and Y. Cao, *Energy Environ. Sci.*, 2021, **14**, 5530-5540.
46 T. Yan, W. Song, J. Huang, R. Peng, L. Huang and Z. Ge, *Adv. Mater.*, 2019, **31**, 1902210.
47 D. Wang, R. Qin, G. Zhou, X. Li, R. Xia, Y. Li, L. Zhan, H. Zhu, X. Lu, H.-L. Yip, H. Chen and C.-Z. Li, *Adv. Mater.*, 2020, **32**, 2001621.
48 L. Zhan, S. Li, T.-K. Lau, Y. Cui, X. Lu, M. Shi, C.-Z. Li, H. Li, J. Hou and H. Chen, *Energy Environ. Sci.*, 2020, **13**, 635-645.
49 C. Zhu, J. Yuan, F. Cai, L. Meng, H. Zhang, H. Chen, J. Li, B. Qiu, H. Peng, S. Chen, Y. Hu, C. Yang, F. Gao, Y. Zou and Y. Li, *Energy Environ. Sci.*, 2020, **13**, 2459-2466.
50 F. Lin, K. Jiang, W. Kaminsky, Z. Zhu and A. K. Y. Jen, *J. Am. Chem. Soc.*, 2020, **142**, 15246-15251.
51 X. Ma, J. Wang, J. Gao, Z. Hu, C. Xu, X. Zhang and F. Zhang, *Adv. Energy Mater.*, 2020, **10**, 2001404.
52 T. Zhang, C. An, P. Bi, Q. Lv, J. Qin, L. Hong, Y. Cui, S. Zhang and J. Hou, *Adv. Energy Mater.*, 2021, **11**, 2101705.
53 A. Zeng, X. Ma, M. Pan, Y. Chen, R. Ma, H. Zhao, J. Zhang, H. K. Kim, A. Shang, S. Luo, I. C. Angunawela, Y. Chang, Z. Qi, H. Sun, J. Y. L. Lai, H. Ade, W. Ma, F. Zhang and H. Yan, *Adv. Funct. Mater.*, 2021, **31**, 2102413.
54 X. Ma, A. Zeng, J. Gao, Z. Hu, C. Xu, J. H. Son, S. Y. Jeong, C. Zhang, M. Li, K. Wang, H. Yan, Z. Ma, Y. Wang, H. Y. Woo and F. Zhang, *Natl. Sci. Rev.*, 2021, **8**, nwaa305.
55 B. Fan, W. Gao, Y. Wang, W. Zhong, F. Lin, W. J. Li, F. Huang, K.-M. Yu and A. K. Y. Jen, *ACS Energy Lett.*, 2021, **6**, 3522-3529.
56 Y. Chang, J. Zhang, Y. Chen, G. Chai, X. Xu, L. Yu, R. Ma, H. Yu, T. Liu, P. Liu, Q. Peng and H. Yan, *Adv. Energy Mater.*, 2021, **11**, 2100079.
57 Y. Chen, F. Bai, Z. Peng, L. Zhu, J. Zhang, X. Zou, Y. Qin, H. K. Kim, J. Yuan, L.-K. Ma, J. Zhang, H. Yu, P. C. Y. Chow, F. Huang, Y. Zou, H. Ade, F. Liu and H. Yan, *Adv. Energy Mater.*, 2021, **11**, 2003141.
58 S. Bao, H. Yang, H. Fan, J. Zhang, Z. Wei, C. Cui and Y. Li, *Adv. Mater.*, 2021, **33**, 2105301.
59 Y. Cai, Y. Li, R. Wang, H. Wu, Z. Chen, J. Zhang, Z. Ma, X. Hao, Y. Zhao, C. Zhang, F. Huang and Y. Sun, *Adv. Mater.*, 2021, **33**, 2101733.
60 Y. Cui, Y. Xu, H. Yao, P. Bi, L. Hong, J. Zhang, Y. Zu, T. Zhang, J. Qin, J. Ren, Z. Chen, C. He, X. Hao, Z. Wei and J. Hou, *Adv. Mater.*, 2021, **33**, 2102420.
61 Y. Xu, Y. Cui, H. Yao, T. Zhang, J. Zhang, L. Ma, J. Wang, Z. Wei and J. Hou, *Adv. Mater.*, 2021, **33**, 2101090.
62 L. Zhan, S. Li, X. Xia, Y. Li, X. Lu, L. Zuo, M. Shi and H. Chen, *Adv. Mater.*, 2021, **33**, 2007231.
63 Y. Zhang, G. Cai, Y. Li, Z. Zhang, T. Li, X. Zuo, X. Lu and Y. Lin, *Adv. Mater.*, 2021, **33**,

2008134.
64 Y. Li, Y. Cai, Y. Xie, J. Song, H. Wu, Z. Tang, J. Zhang, F. Huang and Y. Sun, *Energy Environ. Sci.*, 2021, **14**, 5009-5016.
65 J. Qin, Z. Chen, P. Bi, Y. Yang, J. Zhang, Z. Huang, Z. Wei, C. An, H. Yao, X. Hao, T. Zhang, Y. Cui, L. Hong, C. Liu, Y. Zu, C. He and J. Hou, *Energy Environ. Sci.*, 2021, **14**, 5903-5910.
66 P. Bi, S. Zhang, Z. Chen, Y. Xu, Y. Cui, T. Zhang, J. Ren, J. Qin, L. Hong, X. Hao and J. Hou, *Joule*, 2021, **5**, 2408-2419.
67 Z. Chen, W. Song, K. Yu, J. Ge, J. Zhang, L. Xie, R. Peng and Z. Ge, *Joule*, 2021, **5**, 2395-2407.
68 R. Sun, W. Wang, H. Yu, Z. Chen, X. Xia, H. Shen, J. Guo, M. Shi, Y. Zheng, Y. Wu, W. Yang, T. Wang, Q. Wu, Y. Yang, X. Lu, J. Xia, C. J. Brabec, H. Yan, Y. Li and J. Min, *Joule*, 2021, **5**, 1548-1565.
69 G. Zhang, H. Ning, H. Chen, Q. Jiang, J. Jiang, P. Han, L. Dang, M. Xu, M. Shao, F. He and Q. Wu, *Joule*, 2021, **5**, 931-944.